Competition of halogen bonding and lone pair interactions : cryospectroscopic study of the complexes of (X = F, Cl, Br, and I) and dimethyl ether

On the Competition of C(sp^2)-X···O Halogen Bonding and Lone Pair···π Interactions: A Cryospectroscopic Study of the Complexes of C_2F_3X (X=F, Cl, Br, I) and Dimethyl Ether

Yannick Geboes[a,b], Nick Nagels[a], Balazs Pinter[b], Frank De Proft[b] and Wouter A. Herrebout[a]*

[a] *Department of Chemistry, University of Antwerp, Groenenborgerlaan 171, 2020 Antwerp (Belgium), E-mail: Wouter.herrebout@uantwerpen.be*
[b] *Eenheid Algemene Chemie (ALGC), Member of the QCMM VUB-UGent Alliance Research Group, Vrije Universiteit Brussel, Pleinlaan 2, 1050 Brussels (Belgium)*

Abstract

Inspection of the electrostatic potential of C_2F_3X (X = F, Cl, Br, I) revealed a second electropositive region in the immediate vicinity of the C=C double bond apart from the σ hole of chlorine, bromine and iodine, leading to C(sp^2)-X···Y halogen bonding, through which complexes stabilized by so-called lone pair···π interactions can be formed. Consequently, the experimental studies for the complexes of dimethyl ether with C_2F_3X (X = F, Cl, Br, I) not only allowed to experimentally characterize and rationalize the effects of hybridization on halogen bonding but, for the first time, also allowed the competition of C-X···Y halogen bonding and lone pair···π interactions to be studied at thermodynamic equilibrium. Analysis of the infrared and Raman spectra reveals that in the cryosolutions of dimethyl ether and C_2F_3I, solely the halogen bonded complex is present, whereas C_2F_3Br and C_2F_3Cl give rise to a lone pair···π bonded complex as well as a halogen bonded complex. Mixtures of dimethyl ether with C_2F_4 solely yield a lone pair···π bonded complex. The experimentally derived complexation enthalpies for the halogen bonded complexes are found to be -14.2(5) kJ mol^{-1} for C_2F_3I·DME and -9.3(5) kJ mol^{-1} for C_2F_3Br·DME. For the complexes of C_2F_3Cl with dimethyl ether no experimental complexation enthalpy could be obtained, whereas the C_2F_4·DME complex has a complexation enthalpy of -5.5(3) kJ mol^{-1}. The observed trends have been rationalized with the aid of an interaction energy decomposition analysis (EDA) coupled to a Natural Orbital for Chemical Valence (NOCV) analysis and also using the Non-Covalent Interaction index method.

Keywords: FTIR, Raman, Noncovalent, EDA, NCI, NOCV

1 Introduction

The potential of C-X···Y halogen bonding as a valuable tool to tune key interactions in crystal engineering processes and supramolecular self-assembly, is now well recognized. [1-2] Therefore and because of the awareness of its importance in various biochemical processes, [3] in molecular recognition, [4] and in drug design, [5-6] the phenomenon of halogen bonding has gained a tremendous increase in interest by theoreticians and experimentalists. [7]

The majority of the papers dealing with C-X···Y halogen bonding so far mainly concentrated on halogen donor molecules in which the carbon atoms involved are sp^3 hybridized. As a consequence, little information has been reported on other halogen bonding motifs involving, e.g. sp^2 or sp hybridized carbon atoms. A theoretical study on the influence of the hybridization of the halogen bonded carbon atom has been reported by Zou *et al.*, [8] in which a series of *ab initio* calculations was initiated with the aim of describing the interactions of a variety of halogen donors including, amongst others, HC≡CX, H_2C=CHX and CH_3X (X = Cl, Br and I) with the nitrogen lone pair of ammonia. The results obtained by Zou and co-workers led to the theoretical observation that, within a series of halogen donor molecules, the halogen bonds formed tend to strengthen with increasing *s* character, and led to general assumption that $C(sp^3)$-X < $C(sp^2)$-X < C(sp)-X.

The trends reported by Zou *et al.* [8] are in line with data reported by Li *et al.* [9] suggesting that also for the C-Br···F halogen bonded complexes of CH≡CBr, CH_2=CHBr and CH_3Br with HArF a substantial difference can be observed if the hybridization of the carbon atom is changed. It should however be stressed that, in the same study, the authors also reported a series of calculations for the corresponding fluorinated compounds and that these calculations for CF_3Br and CF_2=CFBr led to complexes with HArF with a very similar interaction energy. The results therefore suggest that, although some calculations reveal that halogen bonding can be affected by the hybridization of the carbon atom involved, this definitely does not lead to a general rule of thumb.

Driven by the fact that $C(sp^2)$-X and C(sp)-X halogen donors show great potential in the field of crystal engineering and supramolecular chemistry, [10-13] and by the fact that the theoretical data reported so far did not lead to an unequivocal description of the intrinsic properties of this kind of interactions, we have initiated an experimental study of the halogen bonded complexes of C_2F_3X (X = F, Cl, Br and I) with dimethyl ether (DME), using infrared and Raman spectroscopy of cryosolutions, i.e. solutions in liquid Argon (LAr) and liquid Krypton (LKr). As reported in previous studies, [14-16] the experimental approaches are supported by *ab initio* calculations, statistical thermodynamics calculations and Monte Carlo simulations. To be able to rationalize the trends observed when passing from $C(sp^3)$-X donors to $C(sp^2)$-X systems, the results presented will be compared with the previous data on the halogen bonded complexes of CF_3X (X = Cl, Br, I) with DME [17] and with the theoretical results for the halogen bonded complexes reported by Zou *et al.* [8] and by Li *et al.* [9]

The choice of the trifluoroethylene derivatives CF_2=CFX (X = Cl, Br, and I) as model systems for the study of $C(sp^2)$-X···Y halogen bonding was further motivated by the observation that, apart from the σ–hole observed for the chlorine, the bromine or the iodine atoms, a second electropositive region was

detected in the immediate vicinity of the C=C double bonds for all four compounds. These regions are clearly visible in the electrostatic potentials shown in Figure 1. These results are also in agreement with the theoretical results reported for other complexes involving hexafluorobenzene and typical Lewis bases, such as water, dimethyl ether and ammonia [18-19] as well as the experimental observation of the $C_6F_6 \cdot H_2O$ complex by Amicangelo *et al.* [20]. Furthermore, in a recent study by Caminati *et al.* [21], the existence of a $C_2F_3Cl \cdot H_2O$ lone pair$\cdots\pi$ bonded complex was demonstrated using Pulsed-Jet Fourier Transform Microwave Spectroscopy. The experimental study for the complexes of DME with C_2F_3X (X = F, Cl, Br, I) therefore does not only allow to experimentally characterize and rationalize the effects of hybridization on halogen bonding but, for the first time ever, also allows the competition of C-X$\cdots$Y halogen bonding and lone pair$\cdots\pi$ interactions to be studied experimentally at thermodynamic equilibrium.

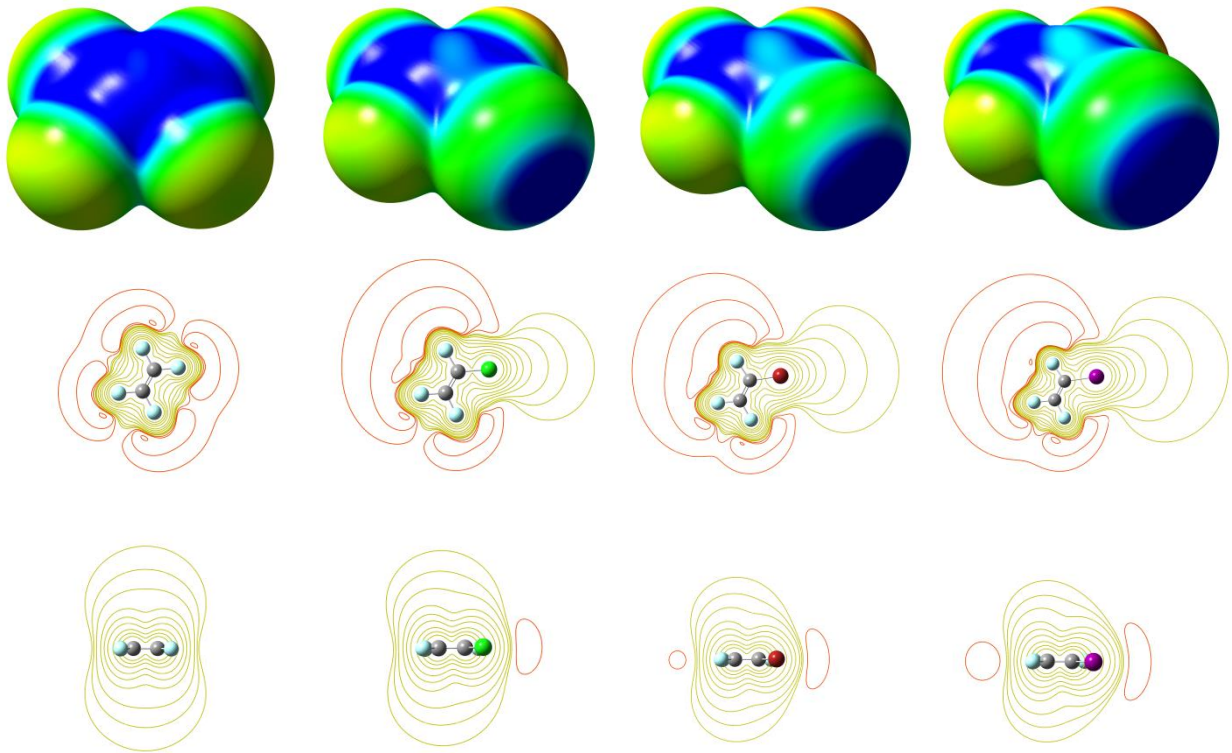

Figure 1: Electrostatic potential (top) of C_2F_4 (left), C_2F_3Cl, C_2F_3Br and C_2F_3I (right) on the molecular surface defined by the 0.001 electrons $Bohr^{-3}$ contour of the electron density, with positive, neutral and negative regions shown in blue, green and red, respectively. Contour plots of the electrostatic potential of the respective halogen donors are also given in red (negative) and green (positive), in the molecular plane (middle) and the plane perpendicular to the first one, along the C=C bond (bottom).

2 Experimental and Computational Details

The samples of tetrafluoroethylene (C_2F_4, 99%) bromotrifluoroethylene (C_2F_3Br, 98%) and chlorotrifluoroethylene (C_2F_3Cl, 99%) were purchased from ABCR. The samples of iodotrifluoroethylene (C_2F_3I, 97%) and dimethyl ether (DME, 99%) were obtained from Lancaster and Sigma Aldrich, respectively. All samples were used without further purification. The solvent gases argon and krypton were supplied by Air Liquide and had a stated purity of 99.9999 % and 99.9995 % respectively.

A Bruker IFS 66v Fourier transform spectrometer, equipped with a Globar source in combination with a Ge/KBr beam splitter and a LN_2-cooled broadband MCT detector, was used to record the infrared spectra. All interferograms were averaged over 500 scans, Blackman-Harris three-term apodized and Fourier transformed with a zero filling factor of 4, to yield spectra with a resolution of 0.5 cm^{-1}. The experimental set-ups used have been described in detail before. [22-24] Liquid cells equipped with wedged Si or ZnSe windows and a path length of 1 cm were used.

Raman spectra were recorded using a Trivista 557 spectrometer consisting of a double f = 50 cm monochromator equipped with 300/900/2000 lines mm^{-1} gratings and an f = 70 cm spectrograph equipped with 500/1800/2400 lines mm^{-1} gratings and a back-end illuminated LN_2 cooled CCD detector. The 514.5 nm line of a Spectra-Physics argon ion laser, 2017-Ar S/N 1665, was used for Raman excitation, the power of the incident laser beam being 0.8 W. Frequencies were calibrated using Ne emission lines, and are expected to be accurate to 0.5 cm^{-1}. The entrance slit to the spectrograph was selected to result in full widths at half-height of the Ne calibration lines between 0.4 and 0.5 cm^{-1}. The experimental set-up, including a liquid cell equipped with four quartz windows at right angles, and the filling procedures have been described before. [25]

For the monomers and the different complexes envisaged, geometry optimizations and harmonic vibrational frequency calculations were performed at the MP2/aug-cc-pVDZ(-PP) level. In addition, complexation energies were derived from single point *ab initio* calculations at the MP2/aug-cc-pVTZ(-PP) level. All *ab initio* calculations were performed using Gaussian09. [26] Corrections for BSSE [27] were accounted for using CP-corrected gradient techniques. [28] The standard aug-cc-pVDZ and aug-cc-pVTZ basis sets were used for hydrogen, carbon, oxygen, fluorine and chlorine. For bromine and iodine, the aug-cc-pVDZ-PP and aug-cc-pVTZ-PP basis sets including small-core energy-consistent relativistic pseudopotentials (PP) were used. The combination of this method and basis set has led to satisfactory results for halogen bonded complexes before [14-15, 29] and, consequently, a similar approach will be used in the present study.

CCSD(T)/CBS (Complete Basis Set) energies were computed using the extrapolation scheme of Truhlar for HF (1) and correlation energies at the MP2 level (2). Furthermore an additional correction term (3) to get CCSD(T) quality results (4) has been introduced analogous to Hobza's method. [30]

$$E_X^{HF} = E_\infty^{HF} + A^{HF} X^{-\alpha} \quad (1)$$

$$E_X^{cor,MP2} = E_\infty^{cor,MP2} + A^{cor,MP2} X^{-\beta} \quad (2)$$

$$\Delta E^{CCSD(T)} = \left| E^{cor,CCSD(T)} - E^{cor,MP2} \right|_{aug-cc-pVDZ(-PP)} \quad (3)$$

$$E_{\infty}^{CCSD(T)} = E_{\infty}^{HF} + E_{\infty}^{corr,MP2} + \Delta E^{CCSD(T)} \quad (4)$$

To evaluate CCSD(T)/CBS energies according to equations (1)-(4), HF/aug-cc-pVDZ(-PP), HF/aug-cc-pVTZ(-PP), MP2/aug-cc-pVDZ(-PP), MP2/aug-cc-pVTZ(-PP) and CCSD(T)/aug-cc-pVDZ(-PP) energies, corrected for the BSSE in all cases, have been computed using Molpro. [31-32] Subsequently, the extrapolation for $E_{¥}^{HF}$ and $E_{¥}^{cor,MP2}$ has been carried out on the X=2, aug-cc-pVDZ(-PP), and X=3, aug-cc-PVTZ(-PP) level using α=3.4 and β=2.2 as proposed by Truhlar. [33]

For all complexes studied, complexation enthalpies in solution $\Delta H°$(LKr,calc) were derived by correcting the theoretical complexation energies ΔE(calc) for zero-point vibrational, thermal and solvent influences. To this end, corrections for thermal effects and zero-point vibrational contributions were obtained using statistical thermodynamics, [34-35] while corrections for solvent effects were obtained using the Monte Carlo Free Energy Perturbation (MC-FEP) approach, as implemented in a locally modified version of BOSS4.0. [36-37]

Ziegler-Rauk type energy decomposition [38-40] and natural orbital for chemical valence (NOCV) analyses were carried out on the MP2/aug-cc-pVDZ(-PP) optimized structures using the PBE[41-42]/TZ2P (small core) functional/basis set combination as implemented in ADF2013.01 [43]. Relativistic effects were taken into account using the Zeroth Order Regular Approximation [44-46] (ZORA), whereas the dispersion energy between monomers was calculated using Grimme's revised DFT-D3 method [47]. Within fragment-based approaches, such the one available in ADF, the complexation energy can be expressed in terms of the strain energy ΔE_{strain} [44, 48-49], which is the energy associated with the geometrical deformation of the fragments from their starting (equilibrium) structure, and the interaction energy between the fragments ΔE_{int} [Eq.(5)].

$$\Delta E = \Delta E_{strain} + \Delta E_{int} \quad (5)$$

Including dispersion, the interaction energy between monomers is evaluated as [38-40, 50]:

$$\Delta E_{int} = \Delta E_{Pauli} + \Delta E_{elst} + \Delta E_{oi} + \Delta E_{disp} \quad (6)$$

where E_{disp} is the dispersion energy and ΔE_{Pauli}, ΔV_{elst} and ΔE_{oi} are the Pauli repulsion, electrostatic interaction and orbital interaction between monomers, respectively. Within this decomposition scheme ΔE_{Pauli} represents the repulsive filled-filled orbital interaction, which is the origin of steric effects [51], whereas ΔE_{oi} corresponds to the stabilizing inter- and intrafragment occupied-vacant orbital mixing upon the formation of the molecule from the predefined fragments.

In the latter process, an important quantity is the deformation density; the Natural Orbitals for Chemical Valence (NOCVs) [52-53], ψ_i, are defined as the eigenvectors that diagonalize this deformation density. In this study the term "NOCV" is simply used for the density deformation, $\Delta\rho_i$, which actually represents a complementary NOCV pair (for details see references 54-55).

$$\Delta\rho_i(r) = \nu_i\left[-\psi_{-i}^2(r) + \psi_i^2(r)\right] \quad (7)$$

NCI plots were computed with the NCIPLOT program [56-57] using MP2/cc-pVTZ(-PP)(-f) wave functions. The NCI method is based on the relationship of the reduced density gradient (*s*) and the electron density (ρ) :

$$s = \frac{1}{2(3\pi^2)^{1/3}} \frac{|\nabla\rho|}{\rho^{4/3}} \qquad (8)$$

The representation of *s* versus ∇ρ shows characteristic peaks at low-density values in the presence of noncovalent interactions due to the annihilation of the density gradient at these points. The strength of the interaction is derived from the density values of the low-gradient spikes, whereas the sign of the second eigenvalue (λ_2) of the electron-density Hessian matrix is used to distinguish between bonded ($\lambda_2 < 0$) and non-bonded ($\lambda_2 > 0$) interactions. [58-60]

3 Results

3.1 *Ab initio* calculations

The isodensity surfaces and contour plots for the electrostatic potential of C_2F_3Cl, C_2F_3Br and C_2F_3I given in Figure 1 show the presence of two electrophilic regions. The first region is located at the outermost portion of the halogen's surface, and allows the formation of C(sp^2)-X···Y halogen bonded complexes. The second region, further noted as the π-hole, is located in the immediate vicinity of the C=C double bond and allows the formation of complexes stabilized by so-called lone pair···π interactions. The σ-hole representing the ability of the molecules to act as halogen donors strongly increases from chlorine to iodine. These results are in line with the results obtained for C(sp^3)-X···Y halogen bonding suggesting that the strength of the interaction increases when replacing the chlorine atom by the more polarizable bromine and iodine atoms. In the case of C_2F_4 no σ-hole is observed and the molecule is expected to interact solely through its π-hole.[61] Inspection of the data in Figure 1 shows that the size of the π-hole remains largely unaffected by the substitution pattern. In contrast to the trends derived for the halogen bonds, it can be conclude that the different lone pair···π interactions will have a similar strength throughout the series of halogen acceptors studied.

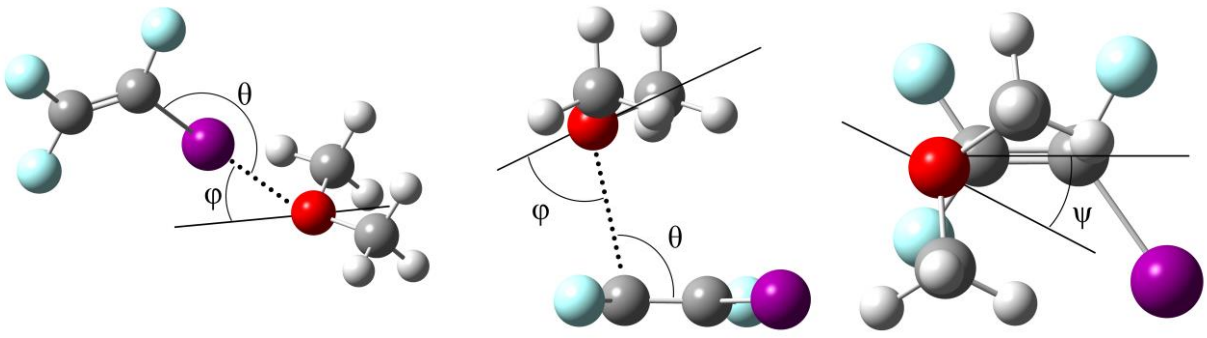

Figure 2: MP2/aug-cc-pVDZ(-PP) equilibrium geometries for the halogen (left) and O···π (middle and right) bonded complex of C_2F_3X (X = F, Cl, Br and I) with DME.

The MP2/aug-cc-pVDZ(-PP) geometries for the complexes of C_2F_3X (X = F, Cl, Br, I) and DME are shown schematically in Figure 2. The intermolecular structural parameters of the C-X···Y halogen and the lone pair···π bonded complexes are summarized in Table 1. For the C-X···Y halogen bonded complexes, the calculations lead to a structure with C_s symmetry. The geometries for the lone pair···π are characterized by C_1 symmetry. For the combination of C_2F_4 with DME, no stationary point was found for the halogen bonded complex and multiple optimization attempts using geometries similar to the expected halogen bonded complex converged to the lone pair···π complex geometry. To allow comparison with data obtained for C(sp^3)-X···Y bonded complexes, the MP2/aug-cc-pVDZ(-PP) geometries obtained for complexes of DME with the trifluoromethyl halides CF_3X (X = Cl, Br or I) are reproduced in Figure S1 of the supporting information. Cartesian coordinates of the monomer and complex geometries are given in Tables S1-S12.

From the data in Figure 2 and Table 1 it can be seen that for all halogen donors studied, a halogen bonded structure is obtained in which the halogen atom is shifted away from the C-O-C bisector, the value of the angle φ between the C-O-C bisector and the line connecting the oxygen and the halogen atoms being approximately 68.0° for C_2F_3Cl, 56.9° for C_2F_3Br and 49.6° for C_2F_3I. These results are in agreement with the values of 66.2°, 56.2° and 49.8° obtained for the complexes of DME with the various trifluoromethyl halides and further support the rabbit ear configuration of the two oxygen lone pairs. [17] A similar tendency, confirming an excellent agreement between the structural parameters obtained for the complexes with CF_3X and C_2F_3X is found for the C-X···O bond angles, the values being 173.0, 176.2 and 177.7 degrees for CF_3X, and 171.4, 175.0 and 176.6 degrees for C_2F_3X, respectively. For the O···π bonded complexes a significant change in torsion angle ψ to 130.0° between the C=C bond and the C-O-C bisector can be noticed for the complex with C_2F_4, indicating that DME has rotated in respect to the C_2F_3X moiety. Furthermore, the decrease of the angle φ between C···O and the C-O-C bisector to 56.5° for the complex with C_2F_4 indicates that the hydrogen atoms of the methyl groups are rotated farther away from the C_2F_3X moiety. The cause of this deviation will be discussed in more detail below.

Table 1: Intermolecular distance R_{eq} (Å), bond angles (°) and the MP2/aug-cc-pVDZ(-PP) ΔE(DZ), MP2/aug-cc-pVTZ(-PP) ΔE(TZ) and CCSD(T)/CBS complexation energies ΔE(CCSD(T)) (kJ mol^{-1}) for the complexes of C_2F_3X (X = F, Cl, Br, I) with DME. For completeness, the corresponding values for the complexes of CF_3X (X = Cl, Br, I) with DME are also given.

O···π bonded	C_2F_4·DME	C_2F_3Cl·DME	C_2F_3Br·DME	C_2F_3I·DME
$R_{eq}=R_{C=C\cdots O}$	2.93	2.91	2.91	2.90
φ	56.52	64.71	63.73	61.90
ψ	130.03	-18.03	-20.91	-21.92
ΔE (DZ) / kJ mol^{-1}	-12.0	-14.1	-14.5	-14.9
ΔE (TZ) / kJ mol^{-1}	-13.0	-15.7	-16.3	-16.9
ΔE (CCSD(T)) / kJ mol^{-1}	-13.7	-15.9	-16.4	-16.7
Halogen bonded	C_2F_3Cl·DME	C_2F_3Br·DME	C_2F_3I·DME	
$R_{eq}=R_{X\cdots O}$	2.97	2.91	2.94	
$\theta_{CX\cdots O}$	171.37	175.04	176.61	
φ	68.04	56.87	49.61	

ΔE (DZ) / kJ mol^{-1}	-11.0	-16.3	-21.8
ΔE (TZ) / kJ mol^{-1}	-11.6	-16.6	-22.3
ΔE (CCSD(T)) / kJ mol^{-1}	-11.7	-16.8	-22.5
Halogen bonded	CF_3Cl·DME	CF_3Br·DME	CF_3I·DME
$R_{eq}=R_{X\cdots O}$	2.96	2.90	2.94
$\theta_{CX\cdots O}$	172.96	176.24	177.71
φ	66.25	56.24	49.80
ΔE (DZ) / kJ mol^{-1}	-11.2	-16.1	-21.5
ΔE (TZ) / kJ mol^{-1}	-11.7	-16.3	-21.9
ΔE (CCSD(T)) / kJ mol^{-1}	-11.9	-16.6	-22.1

The MP2/aug-cc-pVDZ(-PP) and MP2/aug-cc-pVTZ(-PP) complexation energies for the C(sp^2)-X···O bonded and the lone pair···π bonded complexes formed with the various trifluorohaloethenes and the corresponding values for the C(sp^3)-X···O bonded complexes formed with the trifluorohalomethanes are given in Table 1. In agreement with the results reported for CF_3X, a comparison of the different C(sp^2)-X···O bonded complexes revealed a significant increase in complexation energy when moving to the higher halogen atoms at all levels of calculation, the values being -11.6 kJ mol^{-1} for C_2F_3Cl, -16.6 kJ mol^{-1} for C_2F_3Br and -22.3 kJ mol^{-1} for C_2F_3I at the MP2/aug-cc-pVTZ(-PP) level and -11.7 kJ mol^{-1}, -16.8 kJ mol^{-1} and -22.5 kJ mol^{-1} at the CCSD(T)/CBS level, the most accurate method considered. These trends are in line with the general trends deduced from the molecular electrostatic potentials. These values resemble those of the C(sp^3)-X···O bonded complexes and are in line with the data reported by Li *et al.*,[9] suggesting that little or no effects due to changes in hybridization are to be expected for the complexes of HArF and the perfluorinated bromine donors CF≡CBr, CF_2=CFBr.

For all lone pair···π interactions similar values for the complexation energy are obtained, MP2/aug-cc-pVTZ values and the CCSD(T)/CBS for the fluorine, chlorine, bromine and iodine derivatives being -13.0, -15.7, -16.3 and -16.9 kJ mol^{-1} and -13.7, -15.9, -16.4 and -16.7 kJ mol^{-1}, respectively. The similar complexation energies at the MP2/cc-pVTZ(-PP) and CCSD(T)/CBS levels indicate that the effect of CCSD(T) correlation is marginal to MP2. Comparison of these data with the data obtained for the C(sp^2)-X···O halogen bonded complexes reveals an intriguing trend in which the lone pair···π interaction leads to a significantly stronger complex in the case of C_2F_3Cl (-15.9 vs -11.7 kJ mol^{-1}), but gradually loses the competition for C_2F_3Br (-16.4 vs -16.8 kJ mol^{-1}) and C_2F_3I (-16.7 vs. -22.5 kJ mol^{-1}).

The MP2/aug-cc-pVDZ(-PP) harmonic vibrational frequencies and infrared intensities obtained for the monomers and for the complexes under study are listed in Tables S13-S19 of the Supporting Information. From this data it is clear to see that both complex geometries of C_2F_3X·DME (X= Cl, Br, I) can be distinguished in the C=C stretching mode area of the spectrum, as well as the antisymmetrical CF_2 stretch. These vibrational modes will be used in the experimental section to asses which of the complex geometries are found in the noble gas solutions.

In order to differentiate between both geometries in IR and Raman, the complexes should have a sufficient lifetime and tunneling between both should be avoided. To this end, transition point searches

were performed involving the two stable complex geometries of C_2F_3Cl·DME, C_2F_3Br·DME and C_2F_3I·DME. To verify these results, frequency calculations of the proposed first order saddle points were performed to ensure these give rise to only one imaginary frequency. Energy diagrams of the stable geometries and transition points of C_2F_3Cl, C_2F_3Br and C_2F_3I are given in Figures S2, S3 and S4 of the ESI respectively, which clearly show that the transition point is much higher in energy (on average about 8 kJ mol^{-1} higher than the lone pair···π complex), so no tunneling is expected to occur.

3.2 Statistical Thermodynamics and Monte Carlo – Free Energy Perturbation Simulations

To allow comparison with the experimental complexation enthalpies derived from the cryosolutions measurements, the CCSD(T)/CBS complexation energies Δ*E*(calc) were transformed into vapor phase complexation enthalpies Δ*H*°(vap,calc), by accounting for thermal and zero-point vibrational contributions. In addition, to estimate the complexation enthalpies in solutions, further noted as Δ*H*°(LKr,calc), corrections related to the solute-solvent interactions in the solutions were accounted for. The corrections for zero-point vibrational and thermal influences were based on the standard rigid rotor/harmonic oscillator model regularly used in statistical thermodynamics. The calculations were performed at 138 K for Kr and 103 K for Ar, i.e. at the midpoint of the temperature interval used during the experimental study.

Table 2: The values for the CCSD(T)/CBS complexation energies, the calculated vapor phase complexation enthalpies and the calculated liquid krypton and liquid argon complexation enthalpies for the complexes of C_2F_3X (X = F, Cl, Br, I) with DME in kJ mol^{-1}. For completeness, the corresponding experimentally obtained complexation enthalpies, determined in LKr or LAr, and the corresponding values for the halogen bonded complexes of CF_3X (X = Cl, Br, I) with DME, determined in LAr, are also given.[17]

	O···π interaction				Halogen bond			Halogen bond		
	C_2F_4	C_2F_3Cl	C_2F_3Br	C_2F_3I	C_2F_3Cl	C_2F_3Br	C_2F_3I	CF_3Cl	CF_3Br	CF_3I
Δ*E* (CCSD(T))	-13.7	-15.9	-16.4	-16.7	-11.7	-16.8	-22.5	-11.9	-16.6	-22.1
Δ*H*° (vap,calc)	-11.2	-13.4	-13.8	-13.1	-9.2	-14.3	-18.9	-9.9	-14.6	-20.1
Δ*H*° (LKr,calc)	-5.6	-6.4	-6.5	-5.5	-5.9	-10.4	-14.6			
Δ*H*° (LAr,calc)	-5.4							-6.7	-10.7	-16.3
Experimental										
Δ*H*° (LKr)						-9.3(5)	-14.2(5)			
Δ*H*° (LAr)	-5.5(3)							-6.8(3)	-10.2(1)	-15.5(1)

The solvent influences on the complexation enthalpies were derived from the solvation Gibbs energies in LKr, obtained by simulating the immersion of monomers and complexes from the gas phase into the solution, using a Monte Carlo Free Energy Perturbation (MC-FEP) approach. To this end, solvation Gibbs energies of monomers and complexes were estimated at 6 different temperatures varying from 108 to 168 K for LKr and from 73 to 133 K for LAr at a pressure of 28 bar. The enthalpy of

solvation $\Delta_{sol}H$ was then extracted using the expressions $\Delta_{sol}H = \Delta_{sol}G + T\Delta_{sol}S$ and $\Delta_{sol}S = -(\partial \Delta_{sol}G/\partial T)_p$.

The original values for the CCSD(T)/CBS complexation energies, and the calculated values for the vapor phase and solution complexation enthalpies obtained for the different types of complexes of C_2F_3X (X = Cl, Br, I) are collected in Table 2. For completeness, the experimental complexation enthalpies, which are discussed in more detail in the discussion section, and the corresponding values for the halogen bonded complexes of CF_3X (X = Cl, Br, I) with DME, determined in LAr, are also given.[17]

3.3 Vibrational spectra

The vibrational spectrum of DME dissolved in liquid noble gases has been extensively studied. [17, 24, 62-64] The characteristic frequencies and assignments for the trifluorohaloethenes C_2F_3Cl, C_2F_3Br and C_2F_3I observed for solutions in LKr are summarized in Tables S20-22 of the ESI. The assignments for C_2F_4 are based on the harmonic vibrational frequencies derived at the MP2/aug-cc-pVDZ level, and the assignments made by Shimanouchi. [47] For the assignment of the many combination bands and overtones, anharmonic frequency calculations were performed as well. The numbering scheme as proposed by Herzberg was used for the numbering of the fundamental bands. [65] The assignment of the C_2F_3Cl bands is mainly based on the study reported by Gambi et. al. [66] who recently reported a detailed experimental and theoretical study of its harmonic and anharmonic force fields. The assignments for C_2F_3Br and C_2F_3I were based on the harmonic vibrational frequencies derived at the MP2/aug-cc-pVDZ-PP level, as very few spectroscopic studies have yet been performed for these species. [67]

To characterize the different complexes formed between DME and the trifluorohaloethenes, infrared and Raman spectra of solutions in LKr containing mixtures of the acceptor and donor molecules and containing only monomers were recorded, at temperatures between 120 K and 156 K, using different concentrations and ratio for DME and the trifluorohaloethenes.

Inspection of the calculated harmonic vibrational frequencies obtained for the C(sp^2)···O halogen bonded and lone pair···π bonded complexes in Tables S14-S19 shows that for the ν_1 C=C stretching modes in C_2F_3Cl, C_2F_3Br and C_2F_3I the formation of a halogen bond complex with DME leads to a significant red shift of -2.8 , -4.1 and -5.3 cm^{-1}, respectively, while complexation via the π system induces a small blue shift of +2.7, +3.0 and +3.1 cm^{-1}. A similar trend, with red shifts of -4.3, -6.7 and -8.9 cm^{-1} for the halogen bonded complex and blue shifts of +6.7, +7.0 and +7.4 cm^{-1} for the second type of complex is observed for the CF_2 antisymmetric stretching mode ν_2. These modes are predicted to have large infrared and medium Raman intensities in monomers and complexes, as shown in Tables S14 to S19, and were considered as the most promising candidates to experimentally observed and distinguish the complexes formed.

For the lone pair···π bonded complex with C_2F_4, of which the calculated harmonic vibrational frequencies are given in table S13, a slightly different behavior is found for these vibrational modes, with a slightly larger calculated shift of +5.8 cm^{-1} for the IR inactive ν_1 C=C stretching mode and a red shift of

–2.2 cm^{-1} for the CF_2 antisymmetric stretching mode ν_5, which however has B_{1g} symmetry and is also IR inactive, where a blue shift is found for the other lone pair···π bonded complexes.

The C=C stretching regions of the infrared (panels A, C, E and G) and Raman (panels B, D, F and H) spectra obtained for mixed solutions containing DME and C_2F_4 (panels A and B), DME and C_2F_3Cl (panels C and D), DME and C_2F_3Br (panels E and F), and DME and C_2F_3I (panels G and H) are shown in Figure 3. In each panel, the spectrum for the mixed solution, at 120 K, is given in the top trace *a*, while the rescaled spectra of the C_2F_3X and DME monomers, are given in the traces *b* and *c*, respectively. To allow a more thorough analysis, the spectrum of the isolated complex obtained by subtracting rescaled monomer spectra from the spectrum of the mixed solution, is also given (trace *d*). Bands assigned to the 1:1 C(sp^2)···O halogen bonded and the 1:1 lone pair···π bonded complexes are marked with an asterisk (*) and an open circle (°), respectively.

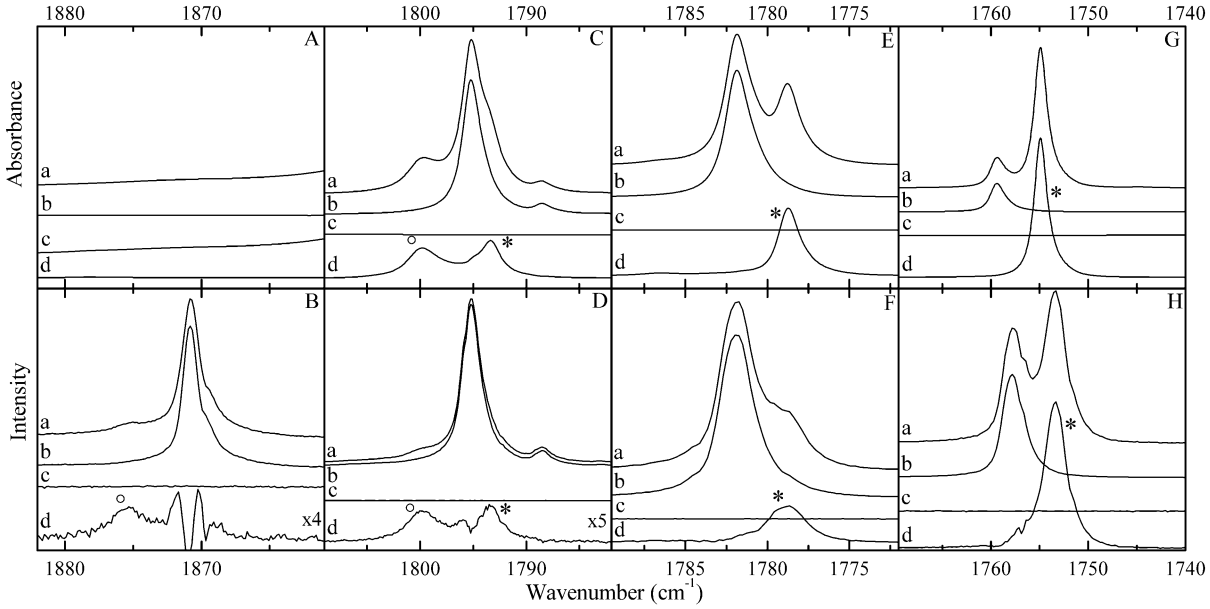

Figure 3: Infrared spectra (panels A, C, E and G) and Raman spectra (panels B, D, F and H) of the $\nu_{C=C}$ spectral region of C_2F_3X (X = F, Cl, Br, I) for solutions of mixtures of DME with C_2F_4 (panels A and B), C_2F_3Cl (panels C and D), C_2F_3Br (panels E and F) and C_2F_3I (panels G and H) dissolved in liquid krypton at 120 K. In each panel, trace *a* represents the mixed solution, while traces *b* and *c* show the solution containing only C_2F_3X or DME, respectively. Trace *d* presents the spectrum of the complex and is obtained by subtracting the rescaled traces *b* and *c* from trace *a*. New bands due to the 1:1 C(sp^2)-X···O halogen bonded and the 1:1 lone pair···π bonded complexes are marked with an asterisk (*) and an open circle (°), respectively.

Since the C=C stretching mode has no IR intensity (as can be seen in Figure 3A) for C_2F_4 due to symmetry restrictions, this region was studied using Raman spectroscopy. For this region, shown in Figure 3B, an additional band, blue shifted by +4.4 cm^{-1} from the C=C stretching mode of the C_2F_4 monomer, can be observed in the spectrum of the mixture. This observation is in good agreement with the predicted blue shift of +5.8 cm^{-1} for the O···π complex. The irregular pattern in the subtracted spectrum near the top of the C_2F_4 monomer band is ascribed to an artefact of the subtraction, and has no physical meaning.

For mixtures of DME with C_2F_3Cl, subtraction of the spectrum of the mixture clearly reveals two additional bands, one blue shifted and one red shifted from the C=C stretching mode band of the monomer, as can be seen in Figures 3C (IR) and 3D (Raman). With experimental shifts of 4.6 cm^{-1} and -1.8 cm^{-1}, these bands can be assigned to the O···π complex and halogen bonded complex respectively. During the subtraction process, an additional feature is observed near the monomer band in both the IR and Raman spectra, making subtraction based on this region difficult. Though the nature of this feature is not fully understood, it is consistent with the presence of 2:1 complex including 2 DME molecules and will be discussed in more detail in a further paragraph.

At first sight, only a red shifted band is observed for the mixture of C_2F_3Br and DME, shown in Figures 3E (IR) and 3F (Raman), which can be ascribed to the presence of halogen bonded complex. However, when the concentration of DME is increased, two weak blue shifted bands can also be observed. A detailed spectrum of this region with an elevated DME concentration is shown in Figure 4. The band with the largest blue shift (+4.4 cm^{-1}) can be ascribed to the presence of a small amount of O···π bonded complex, while the origin of the band with the smaller blue shift is not fully understood.

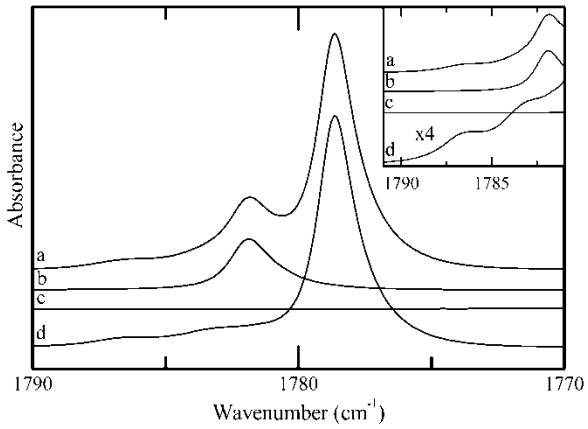

Figure 4: IR spectrum of the C=C stretching region of C_2F_3Br for a mixture with an elevated DME concentration (trace *a*), corresponding rescaled monomer spectra (C_2F_3Br in trace *b* and DME in trace *c*) and the resulting subtracted spectrum, solely containing bands due to complexation (trace *d*). The insert at the right top side of the image shows an enlarged image of the blue shifted bands.

Finally, for mixtures of C_2F_3I with DME, shown in figures 3G (IR) and 3H (Raman), a single complex band with a -4.5 cm^{-1} red shift, assigned to halogen bonded complex, is observed in the C=C stretching region. The observed frequencies, their assignments and their complexation shifts are collected in Tables 3-6.

Table 3: Experimental vibrational frequencies for the monomers and complex, as well as experimental complexation shifts ($\Delta\nu_{exp}$) and MP2/aug-cc-pVDZ calculated complexation shifts ($\Delta\nu_{calc,\,O\cdots\pi}$), in cm^{-1}, for O···π bonded complex (O···π) of C_2F_4 with DME dissolved in LKr at 120 K.

	Assignment	$\nu_{monomer}$	$\nu_{complex}$	$\Delta\nu_{exp}$	$\Delta\nu_{calc,O\cdots\pi}$
C_2F_4	$\nu_1+\nu_9$	3196.6	3198.6	2.0	0.7
	$\nu_1+\nu_{11}$	3045.3	3049.3	4.0	3.4

	ν_1	1870.8	1875.2	4.4	5.8
	ν_9	1330.5	1328.4	-2.1	-5.1
	ν_{11}	1179.5	[a]		-2.5
	ν_2	778.1	777.8	-0.3	-1.6
	ν_{12}	554.7	554.4	-0.3	0.2
	ν_6	549.9			-0.2
	ν_8	505.5			-4.3
	ν_3	395.5			-0.7
DME	ν_1	2990.4	2992.0	1.6	1.5
	ν_{16}	2990.4	2992.0	1.6	-4.7
	$2\nu_3$	2950.7	2952.8	1.1	-1.6
	ν_{12}	2916.6	2921.8	5.2	6.4
	ν_2	2811.9	2814.6	2.7	3.5
	ν_3	1474.9	1475.7	0.8	-0.8
	ν_{18}	1457.7	1458.3	0.6	-0.5
	ν_{13}	1454.9	1455.5	0.6	-0.6
	ν_6	929.4	927.6	-1.8	-3.9

[a] Band could not be observed due to overlap with DME modes.

Table 4: Experimental vibrational frequencies for the monomers and complexes, as well as experimental complexation shifts ($\Delta\nu_{exp}$) and MP2/aug-cc-pVDZ calculated complexation shifts ($\Delta\nu_{calc}$), in cm^{-1}, for the halogen bonded complex (HalB) and O···π bonded complex (O···π) of C_2F_3Cl with DME dissolved in LKr at 120 K. For completeness, the MP2/aug-cc-pVDZ-PP calculated complexation shifts for C_2F_3Cl for the 2:1 complex with 2 DME molecules has also been included.

			HalB			O···π			2:1 complex
	Assignment	$\nu_{monomer}$	$\nu_{complex}$	$\Delta\nu_{exp}$	$\Delta\nu_{calc,}$	$\nu_{complex}$	$\Delta\nu_{exp}$	$\Delta\nu_{calc}$	$\Delta\nu_{calc}$
C_2F_3Cl	ν_1	1795.2	1793.4	-1.8	-2.8	1799.8	4.6	2.7	0.2
	ν_2	1328.1	1323.5	-4.6	-4.3	[a]	> 0	6.7	1.7
	ν_3	1214.3	1212.8	-1.5	-6.2	1212.8	-1.5	-5.9	-9.6
	$2\nu_{10}$	1074.8	1073.4	-1.4	-0.4	[b]		7.4	5.6
	ν_4	1053.7	1053.4	-0.3	-0.6	1054.2	0.5	0.3	-0.3
	ν_5 (^{35}Cl)	691.2	691.1	-0.1	-1.8	691.1	-0.1	-1.0	-2.5
	ν_5 (^{37}Cl)	689.6	689.5	-0.1	-1.8	689.5	-0.1	-1.0	-2.5
	ν_{10}	535.0	534.5	-0.5	-0.2	538.4	3.4	3.7	2.8
	ν_6	516.3	516.5	0.2	0.7	516.5	0.2	0.3	0.9
	ν_7 (^{35}Cl)	462.4	462.0	-0.4	-1.3	462.0	-0.4	-0.7	-1.9
	ν_7 (^{37}Cl)	456.5	456.1	-0.4	-1.3	456.1	-0.4	-0.7	-1.9
DME	ν_1	2990.4	2992.2	1.8	0.5	2992.2	1.8	1.0	
	ν_{16}	2990.4	2992.2	1.8	0.5	2992.2	1.8	-1.2	
	ν_{12}	2916.6	2918.4	1.8	6.2	2918.4	1.8	2.5	
	ν_2	2811.9	2814.8	2.9	3.0	2814.8	2.9	0.3	
	ν_3	1474.9	1475.1	0.2	-1.0	1475.1	0.2	-0.3	
	ν_{18}	1457.7	1458.0	0.3	-1.0	1458.0	0.3	-0.4	
	ν_{13}	1454.9	1455.1	0.2	-0.6	1455.1	0.2	-1.5	
	ν_{19}	1426.3	1427.3	1.0	-0.2	1427.3	1.0	-0.4	
	ν_6	929.4	927.1	-2.3	-5.0	927.1	-2.3	-4.4	

[a] Exact frequency could not be determined due to subtraction artefact.

[b] Band could not be assigned due to overlap with DME.

Table 5: Experimental vibrational frequencies for the monomers and complex, experimental complexation shifts ($\Delta\nu_{exp}$) and MP2/aug-cc-pVDZ-PP calculated complexation shifts ($\Delta\nu_{calc,HalB}$), in cm^{-1}, for the halogen bonded complex of C_2F_3Br with DME dissolved in LKr at 120 K. For completeness, the MP2/aug-cc-pVDZ-PP calculated complexation shifts of the O···π bonded complexes ($\Delta\nu_{calc,O\cdots\pi}$) are also given.

	Assignment	$\nu_{monomer}$	$\nu_{complex}$	$\Delta\nu_{exp}$	$\Delta\nu_{calc,HalB}$	$\Delta\nu_{calc,O\cdots\pi}$
C_2F_3Br	ν_1	1781.8	1778.7	-3.1	-4.1	3.0
	ν_2	1319.8	1313.9	-5.9	-6.7	7.0
	ν_3	1197.2	1191.0	-6.2	-8.3	-6.6
	$2\nu_{10}$	1072.6	1071.4	-1.2	0.7	7.0
	$\nu_5 + \nu_7$ (^{79}Br)	1034.4	1032.1	-2.3	-6.7	-0.4
	$\nu_5 + \nu_7$ (^{81}Br)	1033.3	1031.0	-2.3	-6.7	-0.4
	$2\nu_6$	1018.8	1019.3	0.5	1.2	0.7
	ν_4	1016.6	1016.3	-0.3	-1.2	1.2
	$\nu_5 + \nu_{11}$	998.8	999.0	0.2	5.7	4.3
	$\nu_5 + \nu_8$	980.3	979.4	-0.9	-1.0	-1.1
	ν_5	663.9	663.0	-0.9	-2.1	-0.5
	ν_{10}	535.2	535.1	-0.1	0.3	3.5
	ν_6	509.2	509.7	0.5	0.6	0.3
	ν_7	365.8	363.3	-2.5	-4.6	0.0
	ν_8	311.1	312.1	1.0	1.1	-0.6
	ν_9	162.2	166.0	3.8	5.0	0.4
DME	ν_1	2990.4	2991.8	1.4	2.4	0.6
	ν_{16}	2990.4	2991.8	1.4	2.4	-1.7
	ν_{12}	2916.6	2918.3	1.7	12.3	2.4
	ν_2	2811.9	2817.3	5.4	6.5	0.2
	ν_3	1474.9	1475.2	0.3	-1.6	-0.7
	ν_{18}	1457.7	1458.1	0.4	-1.5	-0.6
	ν_{13}	1454.9	1455.3	0.4	-0.4	-1.8
	ν_{19}	1426.3	1427.1	0.8	-0.1	-0.6
	ν_5	1245.1	1246.6	1.5	0.1	-0.6
	ν_{20}	1172.1	1168.6	-3.5	-7.5	-3.7
	ν_{21}	1099.1	1096.3	-2.8	-5.0	-3.2
	ν_6	929.4	923.7	-5.7	-9.0	-4.4

Table 6: Experimental vibrational frequencies for the monomers and complex, experimental complexation shifts ($\Delta\nu_{exp}$) and MP2/aug-cc-pVDZ-PP calculated complexation shifts ($\Delta\nu_{calc,HalB}$), in cm^{-1}, for the halogen bonded complex of C_2F_3I with DME dissolved in LKr at 120 K. For completeness, the MP2/aug-cc-pVDZ-PP calculated complexation shifts of the O···π bonded complexes ($\Delta\nu_{calc,O\cdots\pi}$) are also given.

	Assignment	$\nu_{monomer}$	$\nu_{complex}$	$\Delta\nu_{exp}$	$\Delta\nu_{calc,HalB}$	$\Delta\nu_{calc,O\cdots\pi}$
C_2F_3I	ν_1	1759.4	1754.9	-4.5	-5.3	3.1
	ν_1 (^{13}C)	1743.8	1739.3	-4.5	-5.3	3.1
	$\nu_4 + \nu_7$	1326.4	1322.0	-4.4	-5.8	2.4
	ν_2	1312.9	1306.4	-6.5	-8.9	7.4
	$2\nu_5$	1302.8	1298.0	-4.8	-4.3	-0.5
	ν_3	1175.5	1167.7	-7.8	-10.2	-5.5
	$\nu_5 + \nu_6$	1156.2	1153.2	-3.0	-1.7	0.1
	$2\nu_{10}$	1080.2	1079.2	-1.0	1.2	7.8
	$2\nu_6$	1013.2	1012.2	-1.0	0.9	0.7
	ν_4	1002.6	1002.2	-0.4	-1.4	1.9
	$\nu_5 + \nu_7$	973.4	968.8	-4.6	-6.6	0.3
	$\nu_5 + \nu_8$	938.7	936.1	-2.6	-3.4	-0.9
	$\nu_{10} + \nu_{11}$	887.4	893.4	6.0	8.9	12.8
	ν_5	651.5	650.4	-1.1	-2.1	-0.2
	ν_{10}	539.4	538.8	-0.6	0.6	3.9
	ν_6	506.7	506.1	-0.6	0.4	0.4
	ν_{11}	349.1	355.4	6.3	8.3	4.7
	ν_7	321.8	318.6	-3.2	-4.4	0.6
	ν_8	287.5	286	-1.5	-1.3	-0.7
	ν_9	145.5	149.4	3.9	5.1	0.7
DME	ν_1	2990.4	2994.0	3.6	4.7	0.0
	ν_{16}	2990.4	2994.0	3.6	4.7	-2.1
	ν_{12}	2916.6	2920.4	3.8	19.6	2.3
	ν_2	2811.9	2820.6	8.7	10.8	-0.1
	ν_{18}	1457.7	1457.5	-0.2	-1.9	-1.0
	ν_{13}	1454.9	1455.0	0.1	-0.2	-2.0
	ν_{19}	1426.3			0.1	-0.7
	ν_5	1245.1	1247.4	2.3	0.6	-0.6
	ν_{20}	1172.1	1166.4	-5.7	-10.8	-4.3
	ν_{21}	1099.1	1093.8	-5.3	-7.5	-3.2
	ν_6	929.4	919.0	-10.4	-14.1	-4.5

It was noted above that apart from the trends observed for the C=C stretching mode, new vibrational bands characteristic for the different types of complexes present should also be expected for the antisymmetric CF_2 stretching mode. The corresponding spectral regions obtained by studying the IR spectra of solutions in LKr, at 120 K, containing mixtures of DME with C_2F_4, C_2F_3Cl, C_2F_3Br and C_2F_3I are shown in Figures 5A, 5B, 5C and 5D, respectively.

For the solutions containing C_2F_3I, Figure 5D, bands assigned to the antisymmetric CF_2 stretching modes in the monomer and in the complex are observed at 1312.9 cm^{-1} and 1306.4 cm^{-1}, respectively. For the solutions containing C_2F_3Br, Figure 5C, the vibrational frequency is red shifted from 1319.8 cm^{-1} in the monomer to 1313.9 cm^{-1} in the complex. The red shifts of -6.5 and -5.9 observed for C_2F_3I and C_2F_3Br again are in striking good agreement with the calculated values -8.9 and -6.7 cm^{-1}. Despite the large concentration of DME, no blue shifted spectral feature due to lone pair···π bonded complex could be observed for the mixture with C_2F_3Br. For the mixtures of DME with C_2F_3Cl, Figure 5B, the subtraction process reveals the presence of a red shifted band (-4.6 cm^{-1}), assigned to the halogen bonded complex, as well as a broader, slightly blue shifted band, ascribed to the lone pair···π complex. However, a small depression is observed in the spectrum resulting from the subtraction process. The origin of this effect remains unclear, but is probably linked to the presence of 2:1 complex, leading to a slight overestimation of the subtraction factor for the C_2F_3Cl monomer. For the mixtures involving C_2F_4, shown in Figure 5A, a single complex band is observed with a red shift of -2.1 cm^{-1}, which is slightly smaller but still consistent with the predicted red shift of -5.1 cm^{-1}. It should however be noted that the antisymmetric CF_2 stretching mode of C_2F_3X (X=Cl, Br or I), ν_2, corresponds to mode ν_5 of C_2F_4, which has no IR intensity. The observed band in the spectra containing C_2F_4, ν_9, corresponds to mode ν_3 of the other trifluorohaloethenes (which lie at a lower frequency due to the presence of a heavier halogen atom), for which both the halogen and lone pair···π bonded complex have a predicted red shift. It is therefore no surprise that the complex band due to the formation of lone pair···π complex in this region is red shifted for C_2F_4, whereas it is blue shifted for C_2F_3Cl.

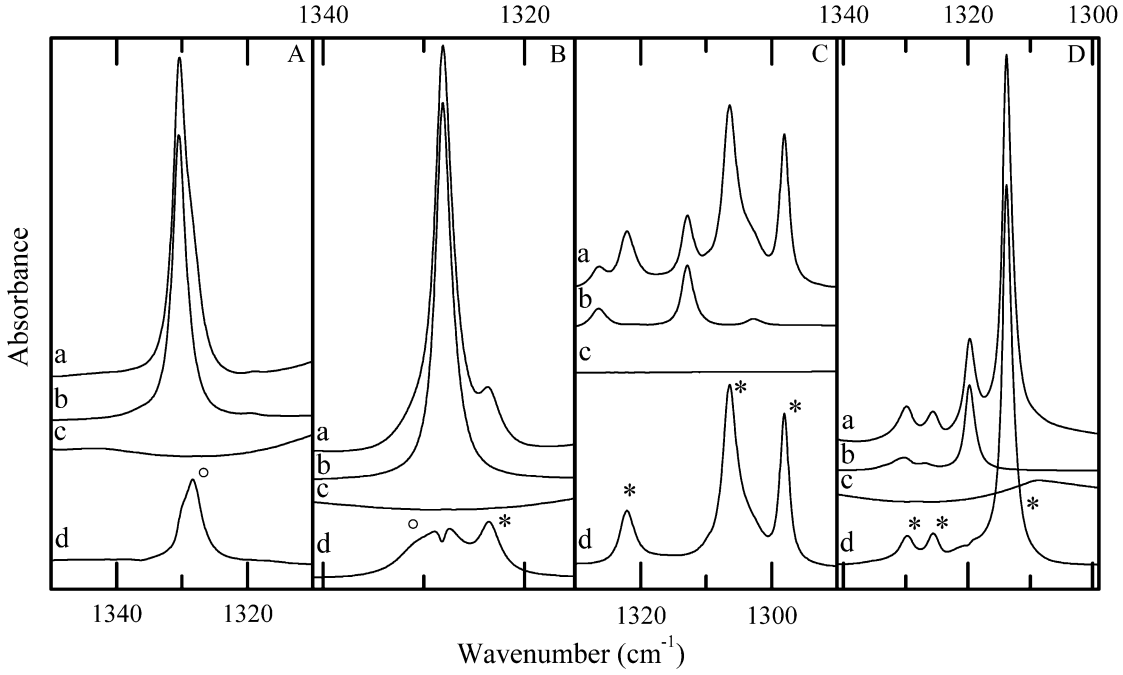

Figure 5: IR spectra of solutions in the ν_2 spectral region of C_2F_3X (X = Cl, Br, I) and the ν_9 spectral region of C_2F_4 of mixtures DME and C_2F_4 (panel A), C_2F_3Cl (panel B), C_2F_3Br (panel C) and C_2F_3I (panel D), dissolved in liquid krypton at 120 K. In each panel, trace *a* represents the mixed solution, while traces *b* and *c* show the solution containing only C_2F_3X or DME, respectively, and trace *d* shows the resulting subtracted spectrum. New bands due to the 1:1 C(sp^2)-X···O halogen bonded and the 1:1 lone pair···π bonded complexes are marked with an asterisk (*) and an open circle (°), respectively.

Finally, a third region for which a distinction between both complexes with C_2F_3Cl can be made is found in the antisymmetric out-of-plane C=C bending mode, ν_{10}, shown in Figure 6. Subtraction yields two distinctive complex bands with shifts of +3.4 cm^{-1} and -0.5 cm^{-1}, which are in excellent agreement with the calculated frequency shifts of +3.7 cm^{-1} for the lone pair···π complex and -0.2 cm^{-1} for the halogen bonded complex.

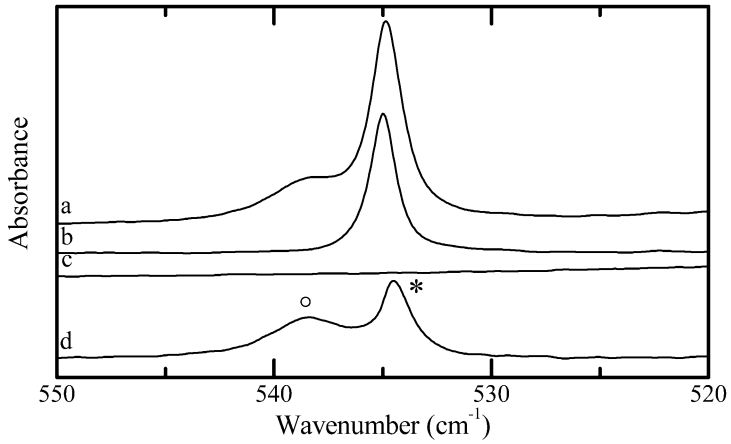

Figure 6: IR spectra of the ν_{10} spectral region of C_2F_3Cl. Trace *a* represents the mixed solution with DME, traces *b* and *c* show the rescale spectra containing only C_2F_3Cl and DME, respectively, while trace *d* shows the resulting subtracted spectrum. New bands due to the 1:1 C(sp^2)-X···O halogen bonded and the 1:1 lone pair···π bonded complexes are marked with an asterisk (*) and an open circle (°), respectively.

3.4 Stoichiometry and Relative Stability

The stoichiometry of the observed complexes was confirmed using concentration studies. During these studies spectra of solutions, containing systematically varied concentrations of the two molecules under study, were recorded at 120 K and the integrated intensities of complex bands $I_{A_mB_n}$ were plotted against the products of the monomer band areas $(I_A)^x(I_B)^y$ for various integer values of *x* and *y*. The analysis is based upon the fact that, under chemical equilibrium conditions, the integrated intensity of a complex band under study $I_{A_mB_n}$ is linearly related to the product of the m^{th} power of the monomer band area I_A and the n^{th} power of the monomer band area I_B.

Typical concentration plots and the corresponding values for the goodness of fit parameter χ^2, confirming the 1:1 stoichiometry of the complexes formed between C_2F_3Br and DME, are presented in Figure S5 of the Supporting Information. Similar analyses leading to the same conclusions were also performed for the complex of C_2F_3I with DME.

The standard complexation enthalpy of the complexes observed was established from temperature studies in which spectra of the mixed solution were recorded as a function of temperature, with the temperature being typically varied between 120 and 156 K. Subsequently, the integrated intensities of the

monomer bands, $I_{C_2F_3X}$ and I_{DME}, and of the complex bands, $I_{complex}$, were used to set up the Van 't Hoff plot. The underlying equation establishes a linear relation between the inverse temperature and the logarithm of the intensity product $I_{complex}/(I_{C_2F_3X} \times I_{DME})$, with a slope equal to $-[\Delta H°(\mathrm{LKr}) + Rb]/R$ and *b* being a correction factor to account for the changes in solvent density upon temperature variation. [68]

Typical Van't Hoff plots obtained for the C(sp^2)-X···O halogen bonded complexes involving C_2F_3I and C_2F_3Br are shown in Figure 7. The average complexation enthalpies for the halogen bonded complexes, obtained by analyzing and averaging out the data for a series of solutions and by correcting the slopes of the different plots for density variations in the temperature intervals used, are -14.2(5) kJ mol^{-1} for C_2F_3I·DME and -9.3(5) kJ mol^{-1} for C_2F_3Br·DME. Even though a small band was observed for the lowest temperatures in the mixture of C_2F_3Br·DME, consistent with the presence of lone pair···π complex, no experimental complexation enthalpy could be obtained for this type of complex.

The spectra of the mixed solutions containing DME and C_2F_3Cl clearly showed the presence of two distinct complexation bands in several regions. However, since both bands were not fully separated in any of the spectral regions, integration of these bands proved to be difficult. Hence, no experimental complexation enthalpies could be obtained for the C_2F_3Cl·DME complexes.

In the case of C_2F_4, a single band was obtained after subtraction, making its integration straightforward. A complexation enthalpy of 5.5(3) kJ mol^{-1} was obtained, which is in agreement with the calculated enthalpy differences of the lone pair···π complex being -5.4 kJ mol^{-1} at the CCSD(T)/CBS level.

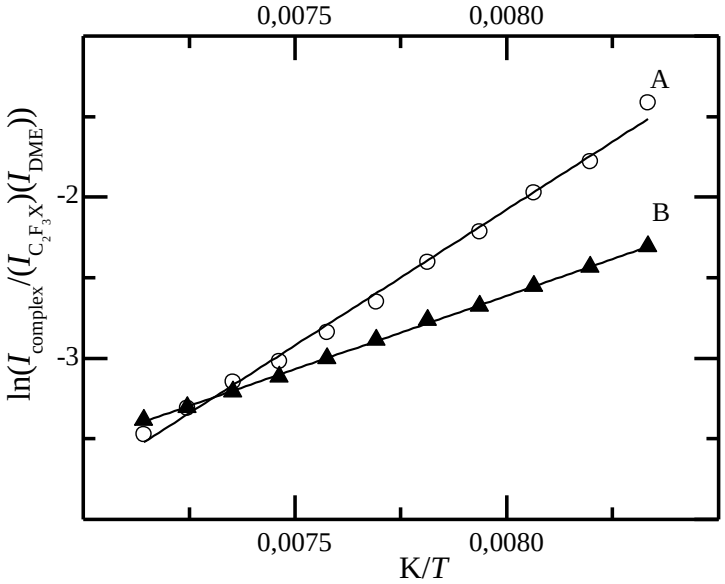

Figure 7: Typical Van't Hoff plots for the halogen bonded complexes of DME with C_2F_3I (A) and C_2F_3Br (B).

3.5 Energy Decomposition Analysis and Non-Covalent Interaction index analysis

Table 7. Interaction energy (ΔE_{int}) and its components, (ΔE_{Pauli}, ΔV_{elst} and ΔE_{oi}) and dispersion (E_{disp}) at the PBE/TZ2P level. The gas phase complexation energy at the MP2/aug-cc-pVTZ(-PP)//MP2/aug-cc-pVDZ(-PP) (ΔE (TZ)) level is also given for comparison. All values are in kJ mol^{-1}.

O···π bonded	C_2F_4·DME	C_2F_3Cl·DME	C_2F_3Br·DME	C_2F_3I·DME
ΔE_{Pauli}	13.2	17.1	17.5	18.0
ΔE_{elst}	-13.3	-14.8	-15.0	-15.4
ΔE_{oi}	-5.6	-7.4	-7.7	-8.1
E_{disp}	-7.9	-10.8	-11.3	-11.5
ΔE_{int}	-13.7	-16.0	-16.4	-17.1
ΔE_{strain}	0.1	0.1	0.1	0.1
ΔE_{DFT}	-13.6	-15.9	-16.3	-17.0
ΔE (TZ)	-13.0	-15.7	-16.3	-16.9
Halogen bonded	C_2F_3Cl·DME	C_2F_3Br·DME	C_2F_3I·DME	
ΔE_{Pauli}	13.4	23.8	37.0	
ΔE_{elst}	-13.6	-23.7	-35.5	
ΔE_{oi}	-6.9	-12.2	-19.5	
E_{disp}	-5.1	-5.5	-5.8	
ΔE_{int}	-12.2	-17.5	-23.8	
ΔE_{strain}	0.2	0.3	0.7	
ΔE_{DFT}	-12.0	-17.2	-23.1	
ΔE (TZ)	-11.7	-16.2	-21.8	

Table 7 shows that the dispersion included DFT-based interaction energies (ΔE_{DFT}) are in excellent agreement with the *ab initio* (MP2/aug-cc-pVTZ) results in general, slightly overestimating it by as much as 0.6 kJ mol^{-1} on average. Moreover, the stability order and trends obtained for ΔE_{int} is the same as for *ab initio* based stabilities (ΔE (TZ)) allowing us to analyze the origin of the stability difference between halogen and O···π-bonded structures in detail using the physically meaningful components of ΔE_{int}, namely steric repulsion (ΔE_{Pauli}), electrostatic interaction (ΔV_{elst}), orbital interaction (ΔE_{oi}) and dispersion (E_{disp}).

As mentioned above, the most striking trend in the complexation energies is the increasing stability of the halogen-bonded systems when going down in the periodic table for the halogen substituent, in contrast to the constant stability of the O···π-bonded complexes, resulting in an inversion of the relative stabilities when going from chlorine (O···π-bonding is stronger) to bromine (both types of interaction are isoenergetic) and to iodine (halogen bonding is stronger). As expected for weak interactions, ΔE_{strain} varies within 0.1 – 0.7 kJ mol^{-1} indicating a negligible contribution from geometry distortions upon complex formation. Rather, it is the interaction energy between monomers, ΔE_{int}, that determines the stability of the studied complexes. For both types of complexes it can be concluded in general that all four

terms contribute notably to the stabilization, and none of the contributing factors really dominates the formation of these systems.

For O···π-bonded systems, except for C_2F_4, all four terms remain relatively constant at about 17 kJ mol^{-1} for steric repulsion, -15 kJ mol^{-1} for electrostatic attraction, -8 kJ mol^{-1} for orbital interaction and -11 kJ mol^{-1} for dispersion, indeed supporting an important electrostatic interaction contribution in line with the modelled molecular electrostatic potentials (Figure 1) and also demonstrating an apparent dispersion contribution. Moreover, such consistency of terms indicates that changing the halogen substituent does not significantly change the acceptor properties of the π* orbital of the C=C bond and, accordingly, the nature of O···π interactions are very similar to each other in these systems. For C_2F_4, whose complex has a characteristically different geometry than the other O···π-bonded systems, steric repulsion between monomers drops by about 5 kJ mol^{-1} with respect to the other O···π-bonded systems, representing a driving force for the structural distortion. All attractive terms, however, also become less attractive in the O···π bonded C_2F_4·DME complex compared to the other O···π-bonded systems.

Since the halogen bond donor properties, both electrostatic and orbital σ-holes, vary with the halogen substituent, the strength of the halogen bonds and accordingly the contributing terms also vary for C_2F_3X systems (X=Cl, Br, and I). When going from Cl to Br and to I, both electrostatic and orbital interactions become more attractive, while dispersion remains constant and relatively unimportant, at about -5 kJ mol^{-1}. Admittedly, steric repulsion increases in the same order, nevertheless, the strength of halogen bonding increases when going down in the periodic table for the halogen substituent X. It is important to notice that the same trends and conclusions have been reached in our former study on $C(sp^3)$-X···B halogen bonded systems (where B is O, N, S and P-based Lewis base) and the proposed rationalization of such behaviour is directly transferable to the $C(sp^2)$-X···O halogen-bonded complexes investigated in this study. Both local softness and hardness of carbon-bonded halogen atoms systematically increase in the order of F < Cl < Br < I and accordingly they tend to develop stronger hard-hard (electrostatics) and stronger soft-soft (charge transfer) interactions that are clearly manifested in the computed ΔV_{elst} and ΔE_{oi} values, respectively. Side-by-side comparison of O···π and X···O bonded isomers pinpoints that dispersion is typically about twice as large for the former than for the latter.

The orbital interaction energy ΔE_{oi} computed in the energy decomposition analysis embodies the stabilization caused by charge transfer between the occupied molecular orbitals on one fragment and the unoccupied molecular orbitals of the other fragment, as well as by the mixing of occupied and virtual orbitals within the same fragment (intrafragment polarization) upon complex formation. There is a density reorganization associated with these processes that can be expressed in NOCVs (eq. (7)-(9)). We found that only one significant NOCV (Figure S6) determines the electron density deformation for O···π and for X···O bond formations, as shown in Figure 8a for representative interactions between C_2F_3Br and DME, with the corresponding charge transfer values and stabilization energies. For halogen bonding the density depletion (orange) – accumulation (green) pattern characterizes an accumulating electron density between the O and X contact atoms originating mostly from DME and at some extent from C_2F_3Br. As already described for other systems, there is a density accumulation not only between the contact atoms

but also on the antibonding orbital of the C-X bond. For O···π interactions the dominant NOCV describes an electron flow from the oxygen's lone pair of DME to the π* orbital of the substituted ethene together with an intrafragment π→ π* charge distribution rearrangement in the latter. The density rearrangement is larger and accordingly more stabilizing upon halogen bond formation than upon O···π bond formation and while it is increasing along the Cl < Br < I series for the former, it remains steady, about 0.09 *e*, for the latter.

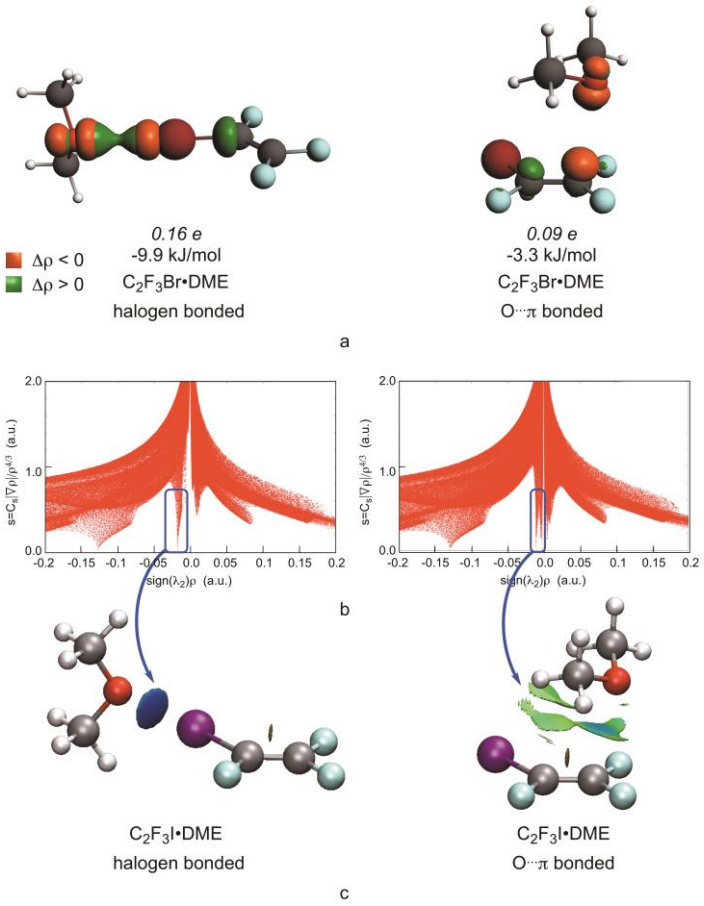

Figure 8: (a) Dominant NOCV with the corresponding density change and associated energy upon halogen (left) and O···π (right) bond formations between C_2F_3Br and DME, (b) plots of the reduced density gradient versus the electron density multiplied by the sign of the second Hessian eigenvalue and (c) gradient isosurfaces (s = 0.5 a.u.) for halogen (left) and lone pair···π (right) bonding between C_2F_3I and DME.

Since the investigated systems exhibit noncovalent interactions it is plausible to apply the NCI framework, introduced by Yang and co-workers to describe noncovalent interactions based on the relationship of the electron density and the reduced density gradient, for the direct comparison of halogen and lone pair···π bonding. This concept was demonstrated to provide valuable insights into many types of weak interactions, including halogen bonding as well as hydrogen bonding, however, to the best of our knowledge, no side-by-side comparison study on halogen vs. lone pair···π bonding was carried out with this technique so far. The results of this analysis for all investigated molecules are given in Figure S7 and Figure S8.

For halogen bonded systems, the plots of the reduced density gradient, *s*, versus ρ for these systems all exhibit the characteristic feature of one spike in the low-energy, low density region, a typical footprint of

noncovalent interactions (Figure 8b, for C_2F_3I·DME interactions). Plotting these points in real space with respect to the geometry of the complex one can easily identify an attractive noncovalent region about midway between contact atoms of the acceptor and the donor (Figure 8c). The *s* versus ρ plots indicate the observed strengthening of halogen bonds when going from C_2F_3Cl to C_2F_3Br and to C_2F_3I (Figure S8), which can be easily monitored with the shift of the characteristic peak towards larger values on the *s* versus ρ plots. The several sharp peaks observed for O···π bonded systems (Figure 8b, right) indicate dispersion in these systems beyond lone pair···π interactions. The plotted NCI index indeed shows extended surfaces between the monomers representing dispersion interactions. The bluish pigmentation (attractive) of the solid green isosurfaces indicates that the strength of the interaction along the C···O axis, which is identified as the lone pair···π interaction, is slightly stronger than the extended dispersion in the Van der Waals regime (green, $\rho < 0.005$ a.u).

4 Discussion

Analysis of the IR and Raman spectra of C_2F_3I with DME has shown that complexation bands, consistent with the formation of a C-I···O halogen bond, are observed in multiple areas of the spectra. No indications of the presence of lone pair···π bonded complex were observed, which is consistent with the large difference in calculated complexation enthalpy in solution between both geometries.

It should, however, come as no surprise that in the mixtures of C_2F_3Br with DME a small band due to the formation of the lone pair···π complex is observed, since the calculated difference in strength in solution between both complexes is a mere 3.9 kJ mol^{-1} (or about 38 % of the strength of the halogen bonded complex), while in a previous study of CHF_2I with trimethylamine, the simultaneous existence of a halogen and hydrogen bond with an experimental enthalpy difference of 4.3 kJ mol^{-1} (23 % of the halogen bonded complex) at similar conditions was proven. [21] The larger difference in relative strength for the present case, however, means that only a very small amount of the weakest (lone pair···π) complex is observed, which is not sufficient for further thermodynamic analysis.

For the solutions containing a combination of C_2F_3Cl and DME, two distinct complex bands can be observed for multiple vibrational modes. The shifts of these bands are in good agreement with the calculated complexation shifts for the halogen bonded complex and lone pair···π bonded complex, thus proving the simultaneous coexistence of both complex geometries in solution. At the lowest temperatures a third small band between both complex bands is observed for the C=C stretching mode, while for the antisymmetric CF_2 stretching the subtraction lead to a small depression in the lone pair···π complex band. As an explanation for these phenomena, frequencies of the 2:1 complex with 2 DME molecules were calculated. When reviewing the shifts of C_2F_3Cl in this 2:1 complex, it can be seen that these are indeed very close to the frequency of the monomer band, which may complicate the subtraction process when using these areas as a reference. Based on the calculated shifts for the 2:1 complex additional measurement were made to study the areas where the 2:1 complex has a shift which is significantly different from both 1:1 complexes and the monomer band. However, no further evidence of the presence of 2:1 complex was found during these measurements.

For the mixtures involving C_2F_4 and DME a single complex band is observed for the IR forbidden C=C stretch using Raman spectroscopy. Furthermore, a single complex band is also observed for ν_9 in FTIR spectra. In both cases, as well as in the case of multiple other (combination) bands, these values are in agreement with the shifts calculated for the lone pair$\cdots\pi$ complex. Furthermore, the experimentally derived complexation enthalpy for these bands is compatible with the theoretically derived value, thus supporting the finding that this is indeed the O$\cdots\pi$ complex. It is also noteworthy that for the O$\cdots\pi$ complex involving C_2F_4 a geometry is calculated that is clearly different from the other complexes since the DME monomer is rotated as compared to the C_2F_3X moiety (angle ψ in Figure 2). This structural distortion can be explained by the lack of a secondary – dispersion like – interaction with the barely polarizable fluorine substituent, in contrast to heavier halogens for which the NCI index clearly indicates weak interactions between the halogen substituent and DME. When this secondary interaction is absent, the C_2F_4·DME complex gets stabilized by the release of filled-filled orbital repulsion (steric effects) between DME and C_2F_4 upon rotation, as can be seen in the energy decomposition analysis. This finding actually highlights that the influence of secondary interactions on the geometry and stability should not be underestimated.

When comparing the complexation enthalpies, a good agreement between experiment and theory can be observed for the halogen bonded complexes of C_2F_3Br·DME and C_2F_3I·DME as well as for the lone pair$\cdots\pi$ bonded C_2F_4·DME complex.

Comparison of the experimental complexation enthalpies for the C_2F_3X and CF_3X halogen bonds with DME reveals similar stabilities when passing from C(sp^3)-X to C(sp^2)-X halogen donors, the former being on average 1.1 kJ mol^{-1} larger. These results are in line with the theoretical data obtained above, and compare favorably with the theoretical observations reported by Li et al. [9] At first sight, this might seem inconsistent with previous studies showing that halogen atoms which are covalently bonded to an atom with higher *s* character tend to form stronger halogen bonds. Even though this is indeed the case for non-perfluorinated cases (e.g. when comparing CH_3X with C_2H_3X and HCCX), for perfluorinated cases, the presence of fluorine atoms in the direct vicinity of the bonding halogen atom, seems to counteract the effect of hybridization. This can be understood by comparing sp^3 CF_3X systems, for which 3 strongly electron withdrawing fluorine atoms are positioned geminal to the halogen atom forming the halogen bond, whereas only one geminal fluorine atom found in the case of C_2F_3X. It is thus not straightforward to say that halogen bonding is enhanced by an increased *s* character of the covalently bonded atom, since effects intrinsically linked to this change in hybridization may counteract this effect completely.

Analysis of the complexes with the NCI program has revealed the presence of secondary interactions for the lone pair$\cdots\pi$ bonded complexes of C_2F_3Cl, C_2F_3Br and C_2F_3I with DME, which are lacking in the complex formed between C_2F_4 and DME. The lack of these secondary interactions explains the deviating geometry of the latter complex, in which DME is rotated compared to the C_2F_4 moiety and the methyl groups are also rotated farther away from C_2F_4.

NOCV analysis characterizes an accumulating electron density between the O and X contact atoms for halogen-bonded systems originating mostly from DME and partially from C_2F_3X, whereas an electron

flow from the oxygen's lone pair of DME to the π* orbital of the substituted ethene together with an intrafragment π→ π* charge distribution rearrangement was revealed in systems exhibiting O···π type interactions. The charge transfer and the associated stabilization are slightly more relevant in the latter species.

5 Conclusions

Inspection of the electrostatic potential of C_2F_3X (X = Cl, Br, I) revealed the presence of two separate electrophilic regions. The first region is situated in the immediate vicinity of the chlorine, bromine and iodine atoms, and, in agreement with the vast literature of σ-hole formation, leads to C(sp^2)-X···Y halogen bonding. The second electrophilic region is related to the π system of the C=C double bond and, in analogy with the interactions between hexafluorobenzene and typical Lewis bases such as water, dimethyl ether and ammonia, can form complexes stabilized by so-called lone pair···π interactions. Furthermore, analysis of the electrostatic surface potential of C_2F_4 yielded only one region of positive electrostatic potential, perpendicular to the molecular plane, through which lone pair···π bonded complexes can be formed.

Experimental studies, supported by *ab initio* calculations, in which the complexes of DME and the various C_2F_3X (X = F, Cl, Br, I) halogen donors formed in cryosolutions are studied using infrared and Raman spectroscopy, reveal that, in cryosolutions, mixtures of DME with C_2F_3I lead solely to halogen bonded complexes. For mixtures of C_2F_3Br with DME, apart from the complex band assigned to the formation a halogen bonded complex, a small secondary band is observed in the C=C stretching area at the lowest temperatures, which is consistent with the formation of a lone pair···π interaction. This band, however, was deemed too small for further analysis. In mixtures containing C_2F_3Cl and DME, two clear complex bands were observed in several spectroscopic areas, which were fully consistent with the simultaneous coexistence of both the halogen bonded and lone pair···π bonded complex in solution. Using spectra recorded at different temperatures between 120 and 156 K, experimental information on the relative stability was obtained by determining the standard complexation enthalpy. For the halogen bonded complexes, the resulting values of -14.2(5) kJ mol^{-1} for C_2F_3I·DME and -9.3(5) kJ mol^{-1} for C_2F_3Br·DME, agree favorably with the predicted values of -14.6 and -10.4 kJ mol^{-1} for the complexation enthalpies in solution, derived from the CCSD(T)/CBS complexation energies. These experimental values are also similar to those reported for the complexes of DME with CF_3I and CF_3Br, with values of -15.5(1) and -10.2(1) kJ mol^{-1} respectively. Therefore, the results reported in this study lead to the first experimental confirmation that, at least for fluorinated halogen donors, the hybridization of the carbon atom involved hardly has an influence on the intrinsic properties of the halogen bond studied, since the number of strong electron withdrawing fluorine atoms geminal to the involved halogen atom is reduced across the sp^3-sp^2-sp series.

Furthermore, the study also enabled a determination of the complexation enthalpy of -5.5(3) kJ mol^{-1} for the C_2F_4·DME lone pair···π bonded complex in LAr, which is also in agreement with the calculated value of -5.4 kJ mol^{-1} derived from the CCSD(T)/CBS calculations.

The experimental studies for the complexes of DME with C_2F_3X (X = Cl, Br, I) not only allowed to experimentally characterize and rationalize the effects of hybridization on halogen bonding but, for the first time ever, also allowed the competition of C-X···Y halogen bonding and lone pair···π interactions to be studied experimentally. Additional information on the complexes of the C_2F_3X (X = F, Cl, Br, and I) halogen donors with other Lewis bases including, amongst others, trimethylamine, allowing further characterization and rationalization of the competition between C-X···Y halogen bonding and lone pair··· π interactions, is the subject of ongoing research activities.

Supporting Information Available: Cartesian coordinates of all monomers and complexes, MP2/aug-cc-pVDZ vibrational frequencies, IR and Raman intensities, characteristic LKr frequencies of C_2F_3X (X= Cl, Br, I), example of CF_3X·DME (X = Cl, Br, I) MP2/aug-cc-pVDZ(-PP) equilibrium geometry, energy diagrams of C_2F_3X·DME (X= Cl, Br, I) complexes including transition states, Stoichiometry plot of the C_2F_3Br·DME halogen bonded complex, dominant NOCV's and NCI plots for all complexes. This material is available free of charge via the Internet at http://pubs.acs.org.

Corresponding Authors:

W.A. Herrebout: e-mail: wouter.herrebout@uantwerpen.be, +32/3.265.33.73

Acknowledgements

Y.G, B.P. and F.D.P. wish to thank the financial support from a Research Program of FWO-Vlaanderen (G.0119.09N), a doctoral fellowship for Y.G. (11O9514N) and a postdoctoral fellowship for B.P. (1279414N). wishes to thank FWO-Vlaanderen for awarding research fellowship. W.H. acknowledges financial support through FWO-Vlaanderen, the Special Research Fund BOF (UA). F.D.P. wishes to acknowledge FWO-Vlaanderen and the Free University of Brussels (VUB) for continuous support to the ALGC research group. The Hercules foundation and the VSC are thanked for generously providing the required CPU resources.

References

1. Metrangolo, P.; Meyer, F.; Pilati, T.; Resnati, G.; Terraneo, G., Halogen Bonding in Supramolecular Chemistry. *Angew. Chem., Int. Ed.* **2008,** *47*, 6114-27.
2. Metrangolo, P.; Resnati, G., Halogen Bonding: Where We Are and Where We Are Going. *Cryst. Growth Des.* **2012,** *12*, 5835-5838.
3. Valadares, N. F.; Salum, L. B.; Polikarpov, I.; Andricopulo, A. D.; Garratt, R. C., Role of Halogen Bonds in Thyroid Hormone Receptor Selectivity: Pharmacophore-Based 3D-QSSR Studies. *J. Chem. Inf. Model.* **2009,** *49*, 2606-2616.
4. Lu, Y. X.; Li, H. Y.; Zhu, X.; Liu, H. L.; Zhu, W. L., Anion Recognition Based on Halogen Bonding: A Case Study of Macrocyclic Imidazoliophane Receptors. *J. Mol. Model.* **2012,** *18*, 3311-3320.
5. Lu, Y. X.; Liu, Y. T.; Xu, Z. J.; Li, H. Y.; Liu, H. L.; Zhu, W. L., Halogen Bonding for Rational Drug Design and New Drug Discovery. *Expert Opin. Drug Discovery* **2012,** *7*, 375-383.

6. Wilcken, R.; Zimmermann, M. O.; Lange, A.; Joerger, A. C.; Boeckler, F. M., Principles and Applications of Halogen Bonding in Medicinal Chemistry and Chemical Biology. *J. Med. Chem.* **2012,** *56*, 1363-1388.
7. Wolters, L. P.; Schyman, P.; Pavan, M. J.; Jorgensen, W. L.; Bickelhaupt, F. M.; Kozuch, S., The Many Faces of Halogen Bonding: A Review of Theoretical Models and Methods. *WIREs Comput. Mol. Sci.* **2014**.
8. Zou, J. W.; Jiang, Y. J.; Guo, M.; Hu, G. X.; Zhang, B.; Liu, H. C.; Yu, Q. S., Ab Initio Study of the Complexes of Halogen-Containing Molecules RX (X=Cl, Br, and I) and NH_3: Towards Understanding the Nature of Halogen Bonding and the Electron-Accepting Propensities of Covalently Bonded Halogen Atoms. *Chem. - Eur. J.* **2005,** *11*, 740-751.
9. Li, Q.-Z.; Li, R.; Jiang, S.-N.; Li, W.-Z.; Cheng, J.-B., The Structure, Properties, and Nature of C–Br···F Halogen Bond Involving HArF: Substitution, Hybridization, and Nonadditivity. *J. Fluorine Chem.* **2012,** *135*, 207-212.
10. Gao, K.; Goroff, N. S., Two New Iodine-Capped Carbon Rods. *J. Am. Chem. Soc.* **2000,** *122*, 9320-9321.
11. Politzer, P.; Murray, J. S.; Concha, M. C., Halogen Bonding and the Design of New Materials: Organic Bromides, Chlorides and Perhaps Even Fluorides as Donors. *J. Mol. Model.* **2007,** *13*, 643-650.
12. Sun, A.; Lauher, J. W.; Goroff, N. S., Preparation of Poly(diiododiacetylene), an Ordered Conjugated Polymer of Carbon and Iodine. *Science* **2006,** *312*, 1030-1034.
13. Yamamoto, H. M.; Maeda, R.; Yamaura, J.-I.; Kato, R., Structural and Physical Properties of Conducting Cation Radical Salts Containing Supramolecular Assemblies Based on P-bis(iodoethynyl)benzene Derivatives. *J. Mater. Chem.* **2001,** *11*, 1034-1041.
14. Hauchecorne, D.; Moiana, A.; van der Veken, B. J.; Herrebout, W. A., Halogen Bonding to a Divalent Sulfur Atom: An Experimental Study of the Interactions of CF_3X (X = Cl, Br, I) with Dimethyl Sulfide. *Phys. Chem. Chem. Phys.* **2011,** *13*, 10204-10213.
15. Hauchecorne, D.; Nagels, N.; van der Veken, B. J.; Herrebout, W. A., C-X···π Halogen and C-H···π Hydrogen Bonding: Interactions of CF_3X (X = Cl, Br, I or H) with Ethene and Propene. *Phys. Chem. Chem. Phys.* **2012,** *14*, 681-690.
16. Hauchecorne, D.; van der Veken, B. J.; Moiana, A.; Herrebout, W. A., The C–Cl···N Halogen Bond, the Weaker Relative of the C–I and C–Br···N Halogen Bonds, Finally Characterized in Solution. *Chem. Phys.* **2010,** *374*, 30-36.
17. Hauchecorne, D.; Szostak, R.; Herrebout, W. A.; van der Veken, B. J., C-X···O Halogen Bonding: Interactions of Trifluoromethyl Halides with Dimethyl Ether. *ChemPhysChem* **2009,** *10*, 2105-2115.
18. Amicangelo, J. C.; Gung, B. W.; Irwin, D. G.; Romano, N. C., Ab Initio Study of Substituent Effects in the Interactions of Dimethyl Ether with Aromatic Rings. *Phys. Chem. Chem. Phys.* **2008,** *10*, 2695-2705.
19. Gung, B. W.; Zou, Y.; Xu, Z. G.; Amicangelo, J. C.; Irwin, D. G.; Ma, S. Q.; Zhou, H. C., Quantitative Study of Interactions Between Oxygen Lone Pair and Aromatic Rings: Substituent Effect and the Importance of Closeness of Contact. *J. Org. Chem.* **2008,** *73*, 689-693.
20. Amicangelo, J. C.; Irwin, D. G.; Lee, C. J.; Romano, N. C.; Saxton, N. L., Experimental and Theoretical Characterization of a Lone Pair-π Complex: Water-Hexafluorobenzene. *J. Phys. Chem. A.* **2013,** *117*, 1336-1350.
21. Nagels, N.; Geboes, Y.; Pinter, B.; De Proft, F.; Herrebout, W. A., Tuning the Halogen/Hydrogen Bond Competition: A Spectroscopic and Conceptual DFT Study of Some Model Complexes Involving CHF_2I. *Chem. - Eur. J.* **2014,** *20*, 8433-8443.
22. Dom, J. J. J.; Michielsen, B.; Maes, B. U. W.; Herrebout, W. A.; van der Veken, B. J., The C–H···π Interaction in the Halothane/Ethene Complex: A Cryosolution Infrared and Raman Study. *Chem. Phys. Lett.* **2009,** *469*, 85-89.

23. Michielsen, B.; Dom, J. J. J.; van der Veken, B. J.; Hesse, S.; Xue, Z.; Suhm, M. A.; Herrebout, W. A., The Complexes of Halothane with Benzene: The Temperature Dependent Direction of the Complexation Shift of the Aliphatic C-H Stretching. *Phys. Chem. Chem. Phys.* **2010,** *12*, 14034-14044.
24. Michielsen, B.; Herrebout, W. A.; van der Veken, B. J., Intermolecular Interactions Between Halothane and Dimethyl Ether: A Cryosolution Infrared and Ab Initio Study. *ChemPhysChem* **2007,** *8*, 1188-1198.
25. Herrebout, W. A.; Nagels, N.; van der Veken, B. J., On the ν_1 ^{CO2}/ 2 ν_2 ^{CO2} Resonance in the Complex of Carbon Dioxide with Dimethyl Ether. *ChemPhysChem* **2009,** *10*, 3054-3060.
26. Frisch, M. J.; Trucks, G. W.; Schlegel, H. B.; Scuseria, G. E.; Robb, M. A.; Cheeseman, J. R.; Scalmani, G.; Barone, V.; Mennucci, B.; Petersson, G. A., et al. *Gaussian 09, Revision D.01*, Gaussian, Inc., Wallingford CT, 2009.
27. Boys, S. F.; Bernardi, F., The Calculation of Small Molecular Interactions by the Differences of Separate Total Energies. Some Procedures with Reduced Errors. *Mol. Phys.* **1970,** *19*, 553-566.
28. Simon, S.; Duran, M.; Dannenberg, J. J., How Does Basis Set Superposition Error Change the Potential Surfaces for Hydrogen Bonded Dimers? *J. Chem. Phys.* **1996,** *105*, 11024-11031.
29. Nagels, N.; Hauchecorne, D.; Herrebout, W. A., Exploring the C-X···π Halogen Bonding Motif: An Infrared and Raman Study of the Complexes of CF_3X (X = Cl, Br and I) with the Aromatic Model Compounds Benzene and Toluene. *Molecules* **2013,** *18*, 6829-6851.
30. Jurecka, P.; Hobza, P., True Stabilization Energies for the Optimal Planar Hydrogen-Bonded and Stacked Structures of Guanine···Cytosine, Adenine···Thymine, and Their 9-and 1-methyl Derivatives: Complete Basis Set Calculations at the MP2 and CCSD(T) Levels and Comparison with Experiment. *J. Am. Chem. Soc.* **2003,** *125*, 15608-15613.
31. Werner, H.-J.; Knowles, P. J.; Knizia, G.; Manby, F. R.; Schütz, M.; Celani, P.; Korona, T.; Lindh, R.; Mitrushenkov, A.; Rauhut, G., et al. *MOLPRO, version 2012.1, A Package of Ab Initio Programs*.
32. Werner, H.-J.; Knowles, P. J.; Knizia, G.; Manby, F. R.; Schütz, M., Molpro: A General-Purpose Quantum Chemistry Program Package. *WIREs Comput. Mol. Sci.* **2012,** *2*, 242-253.
33. Truhlar, D. G., Basis-Set Extrapolation. *Chem. Phys. Lett.* **1998,** *294*, 45-48.
34. Knox, J. H., *Molecular thermodynamics: An introduction to statistical mechanics for chemists*. John Wiley & Sons Ltd., London, 1971.
35. McQuarrie, D. A.; Simon, J. D., *Physical Chemistry: A Molecular Approach*. University Science Books, Sausalito, California, 1997.
36. Delanoye, S. N.; Herrebout, W. A.; van der Veken, B. J., Stabilities of the C-H···O Bonded Complexes of the Haloforms $HCCl_nF_{3-n}$ (n=0-3) with Dimethyl Ether, Oxirane, and Acetone: An Experimental and Theoretical Study. *J. Phys. Chem. A* **2005,** *109*, 9836-9843.
37. Vanspeybrouck, W.; Herrebout, W. A.; van der Veken, B. J.; Lundell, J.; Perutz, R. N., Direct Measurement of the Stability of the Supramolecular Synthon C_6H_6•C_6F_6. *J. Phys. Chem. B* **2003,** *107*, 13855-13861.
38. Ziegler, T.; Rauk, A., On the Calculation of Bonding Energies by the Hartree Fock Slater Method. *Theoret. Chim. Acta* **1977,** *46*, 1-10.
39. Ziegler, T.; Rauk, A., A Theoretical Study of the Ethylene-Metal Bond in Complexes Between Cu^+, Ag^+, Au^+, Pt^0 or Pt^{2+} and Ethylene, Based on the Hartree-Fock-Slater Transition-State Method. *Inorg. Chem.* **1979,** *18*, 1558-1565.
40. Ziegler, T.; Rauk, A., CO, CS, N_2, PF_3, and $CNCH_3$ as σ-donors and π-acceptors. Theoretical Study by the Hartree-Fock-Slater Transitions-State Method. *Inorg. Chem.* **1979,** *18*, 1755-1759.
41. Perdew, J. P.; Burke, K.; Ernzerhof, M., Generalized Gradient Approximation Made Simple. *Phys. Rev. Lett.* **1996,** *77*, 3865-3868.

42. Perdew, J. P.; Burke, K.; Ernzerhof, M., Errata Generalized Gradient Approximation Made Simple. *Phys. Rev. Lett.* **1997,** *78*, 1396-1396.
43. Baerends, E. J.; Autschbach, J.; Bashford, D.; Børces, A.; Bickelhaupt, F. M.; Bo, C.; Boerrigter, P. M.; Cavallo, L.; Chong, D. P.; Deng, L., et al. *ADF2013.01*, Amsterdam (The Netherlands).
44. te Velde, G.; Bickelhaupt, F. M.; Baerends, E. J.; Guerra, C. F.; Van Gisbergen, S. J. A.; Snijders, J. G.; Ziegler, T., Chemistry with ADF. *J. Comput. Chem.* **2001,** *22*, 931-967.
45. van Lenthe, E.; Baerends, E. J.; Snijders, J. G., Relativistic Regular Two-Component Hamiltonians. *J. Chem. Phys.* **1993,** *99*, 4597-4610.
46. van Lenthe, E.; van Leeuwen, R.; Baerends, E. J.; Snijders, J. G., Relativistic Regular Two-Component Hamiltonians. *Int. J. Quant. Chem.* **1996,** *57*, 281-293.
47. Grimme, S.; Antony, J.; Ehrlich, S.; Krieg, H., A Consistent and Accurate Ab Initio Parametrization of Density Functional Dispersion Correction (DFT-D) for the 94 Elements H-Pu. *J. Chem. Phys.* **2010,** *132*, 154104.
48. van Zeist, W. J.; Bickelhaupt, F. M., The Activation Strain Model of Chemical Reactivity. *Org. Biomol. Chem.* **2010,** *8*, 3118-3127.
49. Bickelhaupt, F. M., Understanding Reactivity with Kohn-Sham Molecular Orbital Theory: E2-S_N2 Mechanistic Spectrum and Other Concepts. *J. Comput. Chem.* **1999,** *20*, 114-128.
50. Bickelhaupt, F. M.; Baerends, E. J., Kohn-Sham Density Functional Theory: Predicting and Understanding Chemistry. *Rev. Comput. Chem.* **2000,** *15*, 1-86.
51. Pinter, B.; Fievez, T.; Bickelhaupt, F. M.; Geerlings, P.; De Proft, F., On the Origin of the Steric Effect. *Phys. Chem. Chem. Phys.* **2012,** *14*, 9846-9854.
52. Mitoraj, M. P.; Michalak, A.; Ziegler, T., A Combined Charge and Energy Decomposition Scheme for Bond Analysis. *J. Chem. Theory Comput.* **2009,** *5*, 962-975.
53. Mitoraj, M. P.; Parafiniuk, M.; Srebro, M.; Handzlik, M.; Buczek, A.; Michalak, A., Applications of the ETS-NOCV Method in Descriptions of Chemical Reactions. *J. Mol. Model.* **2011,** *17*, 2337-2352.
54. Pinter, B.; Van Speybroeck, V.; Waroquier, M.; Geerlings, P.; De Proft, F., Trans Effect and Trans Influence: Importance of Metal Mediated Ligand-Ligand Repulsion. *Phys Chem Chem Phys* **2013,** *15*, 17354-17365.
55. Pinter, B.; Broeckaert, L.; Turek, J.; Ruzicka, A.; De Proft, F., Dimers of N-Heterocyclic Carbene Copper, Silver, and Gold Halides: Probing Metallophilic Interactions Through Electron Density Based Concepts. *Chem. - Eur. J.* **2014,** *20*, 734-744.
56. Contreras-Garcia, J.; Johnson, E. R.; Keinan, S.; Chaudret, R.; Piquemal, J. P.; Beratan, D. N.; Yang, W., NCIPLOT: A Program for Plotting Non-Covalent Interaction Regions. *J. Chem. Theory Comput.* **2011,** *7*, 625-632.
57. Johnson, E. R.; Keinan, S.; Mori-Sanchez, P.; Contreras-Garcia, J.; Cohen, A. J.; Yang, W. T., Revealing Noncovalent Interactions. *J. Am. Chem. Soc.* **2010,** *132*, 6498-6506.
58. Lane, J. R.; Contreras-García, J.; Piquemal, J.-P.; Miller, B. J.; Kjaergaard, H. G., Are Bond Critical Points Really Critical for Hydrogen Bonding? *J. Chem. Theory Comput.* **2013,** *9*, 3263-3266.
59. Alonso, M.; Woller, T.; Martin-Martinez, F. J.; Contreras-Garcia, J.; Geerlings, P.; De Proft, F., Understanding the Fundamental Role of π/π, σ/σ, and σ/π Dispersion Interactions in Shaping Carbon-Based Materials. *Chem. - Eur. J.* **2014,** *20*, 4931-4941.
60. Alonso, M.; Pinter, B.; Woller, T.; Geerlings, P.; De Proft, F., Scrutinizing ion-π and ion-σ interactions using the noncovalent index and energy decomposition analysis. *J. Chem. Theory Comput.* **2014,** *DOI: 10.1016/j.comptc.2014.09.033*.
61. Murray, J. S.; Lane, P.; Clark, T.; Riley, K. E.; Politzer, P., σ-holes, π-holes and electrostatically-driven interactions. *J. Mol. Model.* **2012,** *18*, 541-548.

62. Delanoye, S. N.; Herrebout, W. A.; van der Veken, B. J., Improper or Classical Hydrogen Bonding? A Comparative Cryosolutions Infrared Study of the Complexes of $HCClF_2$, $HCCl_2F$, and $HCCl_3$ with Dimethyl Ether. *J. Am. Chem. Soc.* **2002,** *124*, 7490-7498.
63. Van Ginderen, P.; Herrebout, W. A.; van der Veken, B. J., van der Waals Complex of Dimethyl Ether with Carbon Dioxide. *J. Phys. Chem. A* **2003,** *107*, 5391-5396.
64. Herrebout, W. A.; Delanoye, S. N.; Maes, B. U. W.; van der Veken, B. J., Infrared Spectra of the Complexes of Trifluoroethene with Dimethyl Ether, Acetone, and Oxirane: A Cryosolution Study. *J. Phys. Chem. A* **2006,** *110*, 13759-13768.
65. Herzberg, G., *Infrared and Raman Spectra of Polyatomic Molecules*. 12th ed.; D. Van Nostrand Company Inc., Princeton, New Jersey, USA, 1945.
66. Tasinato, N.; Pietropolli Charmet, A.; Stoppa, P.; Giorgianni, S.; Gambi, A., Quantum-Chemical Ab Initio Investigation of the Vibrational Spectrum of Halon 1113 and its Anharmonic Force Field: A Joint Experimental and Computational Approach. *Chem. Phys.* **2012,** *397*, 55-64.
67. Mann, D. E.; Acquista, N.; Plyler, E. K., Vibrational Spectrum of Bromotrifluoroethylene. *J. Chem. Phys.* **1954,** *22*, 1199-1202.
68. van der Veken, B. J., Measurement of Enthalpy Differences in Cryosolutions: Influence of Thermal Expansion. *J. Phys. Chem.* **1996,** *100*, 17436-17438.

Table of Contents graphic